

Dissecting the Hubble tension: Insights from a diverse set of Sound-Horizon-Free H_0 measurements

Ioannis Pantos^{1,*} and Leandros Perivolaropoulos^{1,†}

¹*Department of Physics, University of Ioannina, Greece*

(Dated: January 27, 2026)

The Hubble tension is commonly framed as a discrepancy between local, late-time measurements favoring $H_0 \approx 73 \text{ km s}^{-1} \text{ Mpc}^{-1}$ and early-time, Sound-Horizon-based measurements favoring $H_0 \approx 67 \text{ km s}^{-1} \text{ Mpc}^{-1}$. We challenge this viewpoint by analyzing 88 Sound Horizon Free H_0 measurements, categorized into four classes: Distance Ladder measurements using local calibrators; Local Λ CDM measurements assuming the standard expansion history; Pure Local measurements independent of $H(z)$ shape; and CMB Sound-Horizon-Free measurements using CMB data without the Sound Horizon scale. Our analysis reveals that the 30 Distance Ladder measurements yield $H_0 = 72.73 \pm 0.39 \text{ km s}^{-1} \text{ Mpc}^{-1}$ ($\chi^2_\nu = 0.72$), while the 58 Distance Ladder-Independent/Sound Horizon Free measurements collectively yield $H_0 = 69.37 \pm 0.34 \text{ km s}^{-1} \text{ Mpc}^{-1}$ ($\chi^2_\nu = 0.95$), a 6.5σ tension exceeding the Planck-SH0ES discrepancy. This tension remains significant at a minimum value of 3.9σ after accounting for correlations. Among categories, Local Λ CDM measurements favor the lowest value ($H_0 = 67.61 \pm 0.96 \text{ km s}^{-1} \text{ Mpc}^{-1}$), Pure Local yield an intermediate value ($H_0 = 71.03 \pm 0.69 \text{ km s}^{-1} \text{ Mpc}^{-1}$), and CMB Sound Horizon Free measurements give $H_0 = 69.07 \pm 0.44 \text{ km s}^{-1} \text{ Mpc}^{-1}$. We conclude that the Hubble tension is better characterized as a discrepancy between the Distance Ladder and all other methodologies, rather than an early-vs-late-time split. We also identify a 2.9σ internal tension among Distance Ladder Independent/Sound Horizon Free measurements (noting its sensitivity to categorization choices): analyses assuming Λ CDM systematically recover lower H_0 values by $\sim 3.4 \text{ km s}^{-1} \text{ Mpc}^{-1}$ compared to cosmological-model-independent methods. This suggests either unrecognized systematics in the Distance Ladder or deviations from Λ CDM or both.

I. INTRODUCTION

The determination of the Hubble constant H_0 has reached a level of precision that has arguably transformed a measurement discrepancy into a crisis for the standard cosmological model. The “Hubble tension” refers to the persistent $> 5\sigma$ disagreement between the value inferred from early-Universe probes and that measured from the late-Universe local Distance Ladder.

The standard view frames this tension as a dichotomy between “early” and “late” times. The Planck CMB analysis, assuming Λ CDM, yields $H_0 = 67.4 \pm 0.5 \text{ km s}^{-1} \text{ Mpc}^{-1}$ [1], an inference dependent on the Sound Horizon scale at the drag epoch (r_s). The local Distance Ladder, anchored by geometric measurements and extended via Cepheids to SNe Ia, favors $H_0 = 73.04 \pm 1.04 \text{ km s}^{-1} \text{ Mpc}^{-1}$ [2], reinforced by JWST observations [3] and extended network analyses [4]. If both are accurate, Λ CDM is incomplete, potentially necessitating new physics [5–12].

Various theoretical approaches have been proposed to address the Hubble tension, which can be broadly classified into three categories based on the cosmic epoch at which they introduce new physics [5, 6].

Early-time models attempt to resolve the tension by modifying conditions during the recombination epoch, thereby reducing the Sound Horizon scale r_s that serves

as the standard ruler for CMB-based H_0 inference. Prominent examples include Early Dark Energy (EDE) scenarios and modified gravity theories. However, these approaches face significant challenges: they typically fail to fully resolve the tension, often exacerbate the S_8 tension by enhancing matter clustering, and require considerable fine-tuning of model parameters [13–20].

Late-time models propose deformations in the Hubble expansion history $H(z)$ at low redshifts $z \lesssim 2$, often through dynamical dark energy with an evolving equation of state [21–31]. To understand the implications, it is essential to first outline the theoretical classification of Dark Energy dynamics. The evolution of dark energy is characterized by its equation of state parameter, w , defined as the ratio of its pressure to its energy density ($w = P/\rho$).

In the standard Λ CDM model, this parameter corresponds to a Cosmological Constant and is strictly fixed at $w = -1$. However, dynamical dark energy models are generally categorized into two distinct regimes based on deviations from this value: Quintessence ($-1 < w < -1/3$), which is typically modeled by a scalar field rolling down a potential, and the Phantom regime ($w < -1$), where the fluid exhibits super-negative pressure, leading to an increasing energy density over time [32, 33].

A dynamical evolution in which the parameter $w(z)$ traverses the $w = -1$ boundary is referred to as Phantom Crossing. This transition presents significant theoretical challenges; within the framework of simple perfect fluids or single scalar field models, crossing this boundary typically triggers gradient instabilities or introduces

* i.pantos@uoi.gr

† leandros@uoi.gr

ghost degrees of freedom. Consequently, viable phantom crossing scenarios usually necessitate frameworks beyond standard General Relativity, such as Modified Gravity theories or Effective Field Theory (EFT) approaches, to stabilize the transition [33–36]. Recent analyses incorporating DESI Data Release 2 (DR2) [37] combined with CMB observations favor a Dynamical Dark Energy scenario characterized by a specific phantom crossing behavior. Contrary to simple quintessence models, the data indicate a transition from a phantom-like phase ($w < -1$) in the past to a quintessence-like phase ($w > -1$) at late times, crossing the phantom divide at approximately $z \approx 0.4 - 0.5$, with a present-day value of $w_0 \approx -0.8$.

Crucially, regarding the Hubble tension, this result presents a paradox: due to the geometric anti-correlation between w_0 and H_0 , a present-day value of $w_0 > -1$ implies a lower inferred value for the Hubble constant. Consequently, rather than bridging the gap towards the Distance Ladder value ($H_0 \approx 73 \text{ km s}^{-1} \text{ Mpc}^{-1}$), this specific form of dynamical dark energy risks exacerbating the discrepancy with the high Distance Ladder value. [33, 38–46]. However, it aligns remarkably well with intermediate values: recent work by Zhang et al. using an interacting dark energy model finds $H_0 = 70.00 \pm 1.50 \text{ km s}^{-1} \text{ Mpc}^{-1}$ from CMB+DESI DR2 data (without SH0ES priors), a value consistent with intermediate estimates between Planck and SH0ES [47]. If the DESI evidence for dynamical dark energy is confirmed, the observed shift between ΛCDM -dependent (Category 2) and model-independent (Category 3) measurements transforms from a statistical curiosity into a physical necessity. In this scenario, the Pure Local measurements (Category 3), yielding $H_0 \approx 71 \text{ km s}^{-1} \text{ Mpc}^{-1}$, would emerge as the only methodologically sound Distance Ladder Independent/Sound Horizon Free determinations. Conversely, the lower values found in Category 2 would be interpreted as an artifact of imposing an invalid ΛCDM expansion history on local data. [32, 34–36, 48–53].

Ultralate-time models propose environmental or physical changes at very low redshifts $z \lesssim 0.01$ that could affect the calibration of distance ladder indicators. The G-step model [54–57], which posits a $\sim 4\%$ transition in the effective gravitational constant G_{eff} at $z \approx 0.01$, represents a well-studied example. Related approaches involving screened fifth forces have been explored by Desmond et al. [58–60], who showed that such modifications could systematically affect Cepheid and TRGB distance indicators differently. Alternative explanations within this category include local void scenarios, which posit that our local environment is underdense relative to the cosmic average, leading to an apparent acceleration of the local expansion rate [61–68]. While these models offer mechanisms to reconcile distance ladder and other measurements without modifying early-universe physics, they require fine-tuning and lack complete theoretical justification for the proposed transitions.

However, this “Early vs. Late” characterization may be

oversimplified. It assumes all local measurements favor high H_0 values, an assumption challenged by Distance Ladder Independent/Sound Horizon Free measurements independent of the Cepheid/SN Ia calibration chain. Our recent analysis [69] demonstrated a stark bifurcation: Distance Ladder measurements clustered around $73 \text{ km s}^{-1} \text{ Mpc}^{-1}$, while independent methods statistically favored lower values closer to Planck. This suggests the discrepancy may lie between the distance ladder methodology and other probes, rather than between early and late Universe physics [70]. Indeed, the tension has been shown to have a multidimensional character, with degeneracies between H_0 , Ω_m , and other parameters playing a crucial role [71].

In this work, we present an up-to-date compilation of 88 H_0 measurements published through late-2025, all independent of the CMB Sound Horizon scale. We introduce a four-category classification based on methodology and model dependence: (1) Distance Ladder (30 measurements), (2) Local ΛCDM (33 measurements), (3) Pure Local (cosmological-model-independent, (16 measurements), and (4) CMB Sound Horizon Free (CMB-SHF) (9 measurements). The detailed definitions and classification criteria are presented in Section II B.

The classification follows a systematic decision process (Figure 1): measurements using multi-rung calibration chains are assigned to Category 1; those utilizing CMB data without r_s to Category 4; remaining measurements are assigned to Category 2 or 3 based on whether they assume ΛCDM . The same observational technique can yield measurements in different categories depending on analysis methodology—for example, Megamaser observations with Keplerian models belong to Category 3 [72], while those adopting ΛCDM priors belong to Category 2 [73].

This classification isolates two distinct tensions: the *external tension* between the Distance Ladder and all other methods, and an *internal tension* within these measurements examining whether ΛCDM assumptions systematically shift inferred H_0 values. A comprehensive overview of observational tensions and potential resolutions involving both systematics and fundamental physics has been presented in the CosmoVerse White Paper [74].

This paper is structured as follows: Section II details our data compilation and measurement tables. Section III presents weighted means, reduced chi-squared values, and tension metrics. Section IV discusses model assumption impacts and bimodality in the H_0 distribution. Section V synthesizes these findings and their implications for the Distance Ladder Crisis.

II. DATA COMPILATION AND CATEGORIZATION

To dissect the Hubble tension beyond the traditional “Early vs. Late” dichotomy, we have compiled a comprehensive set of 88 independent measurements of the Hubble constant, updated through late-2025. This com-

pilation builds upon the catalog presented in our previous work [69], significantly expanded to include recent results from James Webb Space Telescope (JWST) calibration campaigns, the third generation of gravitational wave catalogs (GWTC-3), and the latest releases from the Dark Energy Spectroscopic Instrument (DESI) [37].

A. Selection Criteria

Our selection criteria are strictly defined to isolate the impact of the Sound Horizon scale (r_s) and the Distance Ladder methodology:

- 1. Sound Horizon Independence:** We rigorously exclude any measurement that uses the CMB Sound Horizon at the drag epoch as a standard ruler. This excludes standard Baryon Acoustic Oscillation (BAO) inverse Distance Ladder constraints and the standard Planck Λ CDM inference.
- 2. Public Availability:** All measurements are sourced from peer-reviewed journals or preprints available on arXiv.
- 3. Independence of Estimates:** Where multiple analyses utilize the exact same sample (e.g., multiple re-analyses of the same supernova catalog with identical calibration), we select the most recent or representative result to avoid double-counting, unless the methodologies differ significantly in their systematic assumptions.
- 4. Methodological Transparency:** We include only measurements where the original publication clearly states the cosmological assumptions employed, allowing unambiguous category assignment.

B. Classification Methodology

The compiled measurements are classified into four distinct categories based on two primary criteria: (i) reliance on the local Distance Ladder calibration chain, and (ii) dependence on the assumed cosmological model, specifically the shape of the expansion history $H(z)$. The classification follows the decision process outlined in Section I and is determined by the explicit methodological statements in each original publication.

Figure 1 illustrates the classification decision tree schematically. For each measurement, we first assess whether it employs a multi-rung calibration chain (leading to Category 1). If not, we determine whether it utilizes CMB data (leading to Category 4 if Sound-Horizon-Free). For the remaining local measurements, we examine whether the analysis assumes a Λ CDM expansion history (Category 2) or proceeds cosmological-model-independently (Category 3).

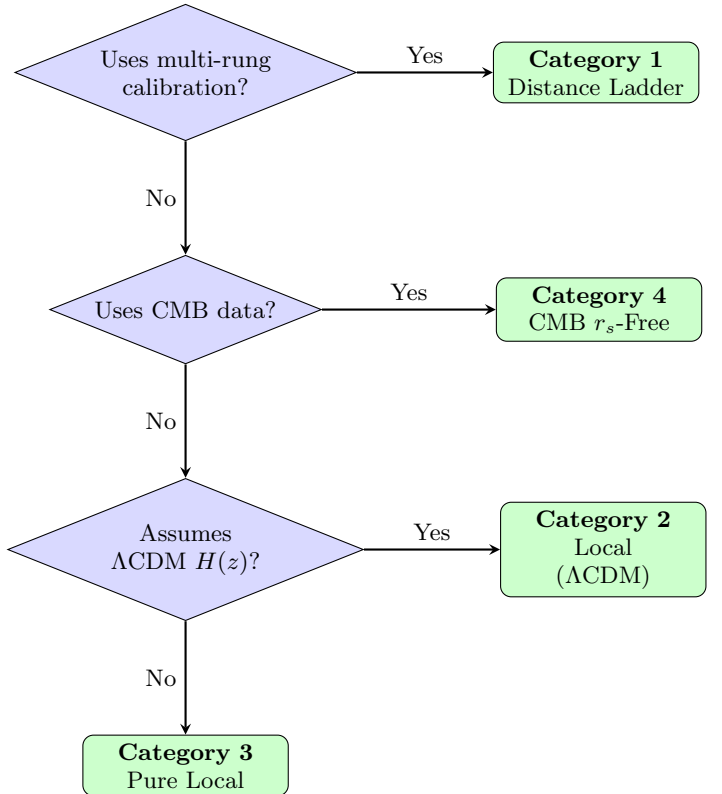


FIG. 1. Decision tree for classifying H_0 measurements into the four categories. Category assignments are based on explicit methodological statements in the original publications.

It is important to emphasize that the same observational technique can yield measurements in different categories depending on the analysis approach adopted by the authors. Table I provides illustrative examples of how specific techniques are distributed across categories based on their methodological implementation.

Throughout this work, we use the term “cosmological-model-independent” (Category 3) to denote measurements that do not assume a specific functional form for the expansion history $H(z)$ —in particular, they do not assume the standard Λ CDM expansion history. This should be understood as independence from cosmological model assumptions rather than complete model independence, as all measurements necessarily rely on certain physical assumptions (e.g., standard astrophysics, the FLRW metric, general relativity). Similarly, we define Distance Ladder-Independent/Sound Horizon Free (DLI-SHF) measurements (Categories 2, 3, and 4) as any H_0 determination that bypasses the traditional three-rung Distance Ladder calibration chain (geometric anchors → Cepheids/TRGB/JAGB/Miras → SNe Ia in the Hubble flow), regardless of whether it probes early or late cosmic times. Some DLI-SHF methods may involve their own calibration procedures (e.g., using cosmic chronometers to calibrate the HII galaxy Hubble diagram), but these do not rely on the standard candle-supernova chain

that defines the Distance Ladder.

TABLE I. Examples of how the same observational technique can be assigned to different categories based on analysis methodology.

Technique	Category (Λ CDM)	2	Category (Cosmological- Model-Independent)	3
Megamasers	Barua (2025): uses Λ CDM $D_A(z)$		Kuo (2013): Keplerian disk only	
Strong Lensing	Shajib (2023): Λ CDM lens model		Du (2023): cosmo- graphic approach	
Gravitational Waves	Abbott (2021): Λ CDM $d_L(z)$		Sneppen (2023): EPM + kilonova	
Cosmic Chronom.	Moresco (2023): Λ CDM fit $H(z)$		Zhang (2022): Gaussian Process	

We now describe each category in detail and present the compiled measurements.

C. Category 1: Distance Ladder Measurements

This category comprises 30 measurements that employ the traditional multi-rung calibration method. These measurements anchor the absolute magnitude of Type Ia supernovae (SNe Ia) in the Hubble flow using local standard candles calibrated by geometric distances. This is the “Late Universe” standard, relying on the fundamental assumption that the physics of calibrators (Cepheids, TRGB, JAGB, Miras) and SNe Ia are uniform across cosmic time and environment.

The three-rung structure proceeds as follows: (1) geometric anchors (Gaia parallaxes, NGC 4258 Megamaser distance, LMC eclipsing binaries) establish absolute distances to nearby calibrators; (2) these calibrators (Cepheids, TRGB, JAGB, Miras) are observed in galaxies that also host SNe Ia, transferring the distance scale; (3) the calibrated SNe Ia absolute magnitude is applied to supernovae in the Hubble flow ($0.023 < z < 0.15$) to infer H_0 .

Our compilation (Table II) includes Cepheid-based measurements and recent JWST updates [3], TRGB-based measurements including CCHP results [75], and alternative calibrators such as JAGB stars, Mira variables, Surface Brightness Fluctuations (SBF), and the Tully-Fisher relation. We also include the galaxy pairwise velocity method [76], which, while methodologically distinct, relies on calibration from distance ladder measurements [77–79].

We note that the Lee [87] JAGB measurement ($H_0 = 67.8 \pm 2.7 \text{ km s}^{-1} \text{ Mpc}^{-1}$) represents a notable outlier within this category, yielding a value consistent with Planck rather than the typical Distance Ladder result. This discrepancy with other JAGB analyses (e.g., Li, Lapuente [86, 88]) appears to originate from differences in the JAGB zero-point calibration and photometric selection criteria, highlighting that even within a single indicator class, methodological choices can significantly impact

TABLE II. **Category 1: Distance Ladder Measurements.** 13 selected representative entries from the 30 measurements in this category. The full table is provided in Appendix A.

Author	Year	H_0	σ	Method
Huang [80]	2019	73.3	4.0	Mira
de Jaeger [81]	2020	75.8	5.1	Cepheids/TRGB + SNe II
Khetan [82]	2021	70.5	4.1	SBF
Freedman [83]	2021	69.8	1.7	TRGB (CCHP)
Kenworthy [84]	2022	73.1	2.5	Two-rung ladder
Scolnic [85]	2023	73.22	2.06	TRGB (SH0ES calibrators)
Li [86]	2024	74.7	3.1	JAGB + SNe Ia
Lee [87]	2024	67.8	2.7	JAGB + SNe Ia
Lapuente [88]	2025	72.61	1.69	TRGB+JAGB+Ceph.+SNe Ia (twins)
Jensen [89]	2025	73.8	2.4	TRGB
Riess [3]	2025	73.49	0.93	Cepheids (JWST)
Bhardwaj [90]	2025	73.06	2.6	Mira
Newman [91]	2025	75.3	2.9	TRGB + SNe Ia

the inferred H_0 . A critical recent addition to this category is the analysis by Ruiz-Lapuente et al. [88], which utilizes the “SNe Ia twins” method calibrated via both TRGB and JAGB. Notably, their specific calibration using JAGB yields $H_0 = 72.34 \text{ km s}^{-1} \text{ Mpc}^{-1}$, while their TRGB determination gives $72.54 \text{ km s}^{-1} \text{ Mpc}^{-1}$. In our compilation (Table II), we have adopted the value $H_0 = 72.61 \pm 1.69 \text{ km s}^{-1} \text{ Mpc}^{-1}$, which represents the weighted average across the different methodological combinations presented in their work. This independent confirmation of high H_0 values using alternative calibrators is particularly significant as it directly challenges previous lower estimates ($H_0 \sim 69.8 \text{ km s}^{-1} \text{ Mpc}^{-1}$) historically associated with the CCHP program. It suggests that the previously reported discrepancies between Cepheids and other local calibrators of the Distance Ladder may have been overstated, implying that unrecognized systematics in the specific calibration or sample selection of earlier CCHP analyses—rather than the indicators themselves—may account for the lower values. Consequently, this result reinforces the internal consistency of Category 1, further isolating the Distance Ladder methodology from the rest of the cosmological probes.

D. Category 2: Local (Λ CDM Assumption)

This category includes 33 measurements that bypass the Distance Ladder but infer H_0 by explicitly assuming the standard Λ CDM expansion history:

$$H(z) = H_0 \sqrt{\Omega_m(1+z)^3 + 1 - \Omega_m}. \quad (1)$$

While these methods probe the local Universe (typically $z < 1.5$), they rely on this model to map observables—such as time delays, luminosity distances, dispersion measures, or angular diameter distances—to H_0 . The key criterion for inclusion in this category is that the original analysis *explicitly assumes* the functional form of Eq. (1), often with Ω_m fixed to a fiducial value (typically $\Omega_m \approx 0.3$) or marginalized over a narrow prior.

This category includes:

- **Gravitational Wave Standard Sirens:** Both bright sirens (with EM counterparts, e.g., GW170817 [92]) and dark sirens (using galaxy catalogs for redshift inference [93, 94]), where the luminosity distance $d_L(z)$ is computed assuming Λ CDM.
- **Strong Lensing Time Delays:** Analyses where the cosmological model enters both the time-delay distance calculation and often the lens mass modeling [95–97].
- **Fast Radio Bursts:** Measurements using the dispersion measure–redshift relation interpreted under Λ CDM assumptions for the intergalactic medium [98, 99].

TABLE III. **Category 2: Local (Λ CDM Assumption).** 12 selected representative entries from the 33 measurements in this category. The full table is provided in Appendix A

Author	Year	H_0	σ	Method
Wu [98]	2021	68.8	4.7	FRBs
Shajib [95]	2023	77.1	7.2	Lensing (TDCOSMO)
Napier [100]	2023	74.1	8.0	Cluster Lenses
Kelly [96]	2023	66.6	3.7	Lensed SN Refsdal
Liu [101]	2023	59.1	3.6	Cluster Lensed Quasar
Martinez [102]	2023	74.0	11.2	Time-Delay Cosmography
Pascare [103]	2024	71.8	8.7	Lensed SN H0pe (JWST)
Yang [104]	2024	74.0	7.4	FRBs w/ Scattering
Piratova [99]	2025	65.1	7.4	FRBs (MLE)
Beirnaert [94]	2025	79.0	9.0	GW Dark Sirens
Birrer [97]	2025	71.6	3.6	TDCOSMO Strong Lensing
Pierel [105, 106]	2025	66.9	9.8	SN Encore Time Delays

E. Category 3: Pure Local (Cosmological-Model Independent)

This category represents the cleanest test of the Distance Ladder, as it comprises 16 measurements that determine H_0 geometrically or via direct measurement of the expansion rate, *without* assuming a specific functional form for $H(z)$. These measurements are either:

- **Purely geometric:** Relying on Keplerian dynamics or light-travel-time arguments that are independent of the global cosmological model (e.g., Megamaser disk modeling [72, 107]).
- **Direct $H(z)$ measurements:** Cosmic chronometers measure $H(z) = -\frac{1}{1+z} \frac{dz}{dt}$ directly from the differential aging of massive, passively evolving galaxies, providing cosmological-model-independent determinations of the expansion rate at various redshifts [108]. To extract H_0 , two main approaches have been employed: (i) Gaussian Process reconstruction of $H(z)$ combined with a cosmographic expansion of the luminosity distance in the Hubble

flow ($0.02 < z < 0.15$), (ii) using cosmic chronometers to calibrate the H II galaxies Hubble diagram, which in turn anchors Type Ia supernovae at low redshift via Hubble’s law [109]. Both methods avoid assumptions about the underlying cosmological model beyond the FLRW metric.

- **Cosmographic approaches:** Analyses that expand $H(z)$ or $d_L(z)$ in Taylor series around $z = 0$, avoiding assumptions about the energy content of the Universe [110].
- **Expanding photosphere methods:** Geometric distance determinations from supernovae using photospheric velocity and angular size evolution [111, 112].

The key distinction from Category 2 is that these analyses do *not* assume the validity of Eq. (1). For Megamaser measurements, we include in this category only those analyses that rely purely on Keplerian disk modeling without adopting Λ CDM-based peculiar velocity corrections or external distance priors tied to the Distance Ladder.

TABLE IV. **Category 3: Pure Local (Cosmological-Model Independent).** 9 representative measurements in this category, representing the cosmological-model-independent local determinations of H_0 . The full table is provided in Appendix A

Author	Year	H_0	σ	Method
Kuo [72]	2013	68.0	9.0	Megamasers (MCP)
Gao [107]	2015	66.0	6.0	Megamasers
Zhang [109]	2022	65.9	3.0	CC + HII
Du [110]	2023	71.5	3.8	TD Lenses + GRBs
Sneppen [111]	2023	67.0	3.6	EPM + Kilonovae
Li [113]	2024	66.3	3.7	Lensing Bias Correction
Vogl [112]	2024	74.9	2.7	SNe II (Tailored EPM)
Song [114]	2025	70.4	6.9	GW + SGL Calibration
Favale [115]	2025	68.8	3.0	Cosmic Chronometers

We highlight that this category exhibits significant internal heterogeneity. Notably, the Vogl [112] tailored EPM measurement ($H_0 = 74.9 \pm 2.7 \text{ km s}^{-1} \text{ Mpc}^{-1}$) strongly favor the Distance Ladder value, while most cosmic chronometer measurements favor lower values. This heterogeneity will be discussed further in Section IV.

F. Category 4: CMB Sound-Horizon-Free (CMB–SHF)

The final category includes 9 measurements that utilize early-Universe data (primarily CMB) but specifically avoid the Sound Horizon r_s as a standard ruler. Instead, these methods rely on alternative physical scales that are calibrated independently of pre-recombination acoustic physics:

- **Matter-radiation equality scale (k_{eq}):** The comoving wavenumber corresponding to the horizon

size at matter-radiation equality provides a standard ruler that depends on $\Omega_m h^2$ and $\Omega_r h^2$ but is independent of r_s [116, 117].

- **BAO without r_s priors:** Analyses that use BAO peak positions but treat r_s as a free parameter, constraining H_0 through the shape of $H(z)$ rather than absolute calibration [118].
- **Sunyaev-Zel'dovich (SZ) effect:** Combining SZ decrements with X-ray observations of galaxy clusters to infer angular diameter distances independent of r_s [119, 120].

TABLE V. **Category 4: CMB Sound Horizon Free.** All 9 measurements in this category, utilizing early-Universe data without the Sound Horizon scale.

Author	Year	H_0	σ	Method
Reese [119]	2003	61.0	18.0	SZ Effect
Philcox [116]	2022	64.8	$^{+2.2}_{-2.5}$	BAO scale, Matter-rad. eq.
Colaco [120]	2023	67.2	6.1	SZ + X-ray
Pogosian [118]	2024	68.05	0.94	BAO-pre DESI (No r_s)
Pogosian ^a [121]	2025	69.37	0.65	BAO-DESI DR2 (No r_s)
Bahr-Kalus [117]	2025	65.2	5.6	DESI Turnover Scale
Garcia [122]	2025	70.03	0.97	BAO-DESI DR2 + θ^* + A_s (No r_s)
Zaborowski [123]	2025	70.8	$^{+2.0}_{-2.2}$	BAO-DESI + θ^* (No r_s)
Krolewski [124]	2025	69.0	2.5	DESI + CMB (No r_s)

^a Private communication.

We note that this category includes two entries from Pogosian et al. [118, 121], corresponding to analyses using DESI and pre-DESI BAO data respectively. While these share a common methodology, they utilize substantially different datasets and thus provide partially independent constraints.

G. Summary of Classification

Table VI summarizes the four categories and their key characteristics. The complete measurement tables with extended methodological information are provided in Appendix A.

TABLE VI. Summary of the four measurement categories.

Cat.	Description	N	Uses Ladder?	Assumes Λ CDM?
1	Distance Ladder	30	Yes	No
2	Local (Λ CDM)	33	No	Yes
3	Pure Local	16	No	No
4	CMB-SHF	9	No	Yes*

*Category 4 assumes Λ CDM for $H(z)$ shape but avoids the Sound Horizon r_s .

III. STATISTICAL ANALYSIS AND RESULTS

In this section, we present a detailed statistical analysis of the H_0 measurements classified in Section II.

We utilize the inverse-variance weighted mean to determine the central value for each category and the reduced chi-squared statistic (χ^2_ν) to assess internal consistency. We explicitly quantify the tension between the Distance Ladder (Category 1) and the various subsets of Sound-Horizon-Free measurements, concluding with a comparison against the combined ensemble of all Distance Ladder Independent/Sound Horizon Free (DLI-SHF) methods. We also compare our results with our previous analysis [69] to assess the evolution of the tension landscape.

A. Methodology

For a set of N independent measurements $\{H_{0,i} \pm \sigma_i\}$, the weighted mean \hat{H}_0 and its standard error $\sigma_{\hat{H}_0}$ are calculated as:

$$\hat{H}_0 = \frac{\sum_{i=1}^N w_i H_{0,i}}{\sum_{i=1}^N w_i}, \quad \sigma_{\hat{H}_0} = \left(\sum_{i=1}^N w_i \right)^{-1/2}, \quad (2)$$

where the weights are given by $w_i = 1/\sigma_i^2$. This estimator minimizes the variance for Gaussian-distributed errors.

To evaluate whether the variation within a category is consistent with the reported uncertainties, we compute the reduced chi-squared:

$$\chi^2_\nu = \frac{1}{N-1} \sum_{i=1}^N \frac{(H_{0,i} - \hat{H}_0)^2}{\sigma_i^2}. \quad (3)$$

In cases of asymmetric errors, the following Equation is adopted for computations involving the mean or a unified error value:

$$\sigma = \sqrt{\frac{(\sigma^+)^2 + (\sigma^-)^2}{2}} \quad (4)$$

The interpretation of χ^2_ν provides important diagnostic information:

- $\chi^2_\nu \approx 1$: Good internal consistency; the scatter is consistent with reported uncertainties.
- $\chi^2_\nu \gg 1$: Underestimated errors, unrecognized systematics, or genuine physical scatter.
- $\chi^2_\nu \ll 1$: Overestimated errors, unaccounted correlations between measurements, or possible publication bias toward a consensus value.

The statistical tension between two independent estimates A and B is quantified in terms of standard deviations (n_σ) as:

$$n_\sigma = \frac{|\hat{H}_{0,A} - \hat{H}_{0,B}|}{\sqrt{\sigma_A^2 + \sigma_B^2}}. \quad (5)$$

We note that this tension metric assumes statistical independence between the two samples. In practice, correlations exist within each category due to shared calibration data, common analysis frameworks, and overlapping

samples. We address the impact of these correlations in Appendix C, where we show that accounting for realistic correlation structures reduces the tension significance but does not qualitatively alter our conclusions.

B. Weighted Mean Statistics by Category

The statistical results for the four categories defined in Section II are summarized in Table VII. For comparison, we also include the results from our previous analysis [69], which employed a binary classification scheme (Distance Ladder vs. Distance Ladder Independent/Sound Horizon Free).

TABLE VII. Statistical Summary of Sound-Horizon-Free Categories. The weighted mean H_0 ($\text{km s}^{-1} \text{Mpc}^{-1}$), uncertainty, reduced chi-squared (χ_ν^2), and tension relative to Category 1 (Distance Ladder). The bottom section shows the combined DLI-SHF results and, for comparison, the results from our 2024 analysis [69].

Category	N	$H_0 \pm \sigma$	χ_ν^2	Tension
1. Distance Ladder	30	72.73 ± 0.39	0.72	—
2. Local (ΛCDM)	33	67.61 ± 0.96	0.80	4.9σ
3. Pure Local	16	71.03 ± 0.69	0.77	2.2σ
4. CMB-SHF	9	69.07 ± 0.44	0.89	6.1σ
<i>Combined (2+3+4)</i>	58	69.37 ± 0.34	0.95	6.5σ
<i>Corr.-adjusted (2+3+4)</i>	58	69.52 ± 0.42	—	3.9σ
<i>Comparison with Perivolaropoulos (2024) [69]:</i>				
2024 Distance Ladder	20	72.8 ± 0.5	0.51	—
2024 DLI-SHF	33	68.3 ± 0.5	0.95	$\sim 5\sigma$

To visualize the distinct behaviors of these categories, we present the Gaussian probability distributions in Figure 2. This Figure illustrates the probability density functions for each of the four subgroups, offering a clear visual representation of the tensions quantified in Table VII.

1. Category 1: Distance Ladder ($H_0 = 72.73 \pm 0.39 \text{ km s}^{-1} \text{Mpc}^{-1}$)

The 30 measurements comprising the Distance Ladder category yield a weighted mean of $H_0 = 72.73 \pm 0.39 \text{ km s}^{-1} \text{Mpc}^{-1}$. As shown in Figure 2, this category forms a sharp, narrow peak that is clearly separated from the other distributions.

The reduced chi-squared $\chi_\nu^2 = 0.72$ indicates good internal consistency, with the scatter being slightly smaller than expected from the reported uncertainties. This value is notably higher than our 2024 analysis ($\chi_\nu^2 = 0.51$), suggesting that the expanded data—which now includes measurements with greater methodological diversity (e.g., JAGB, Miras, pairwise velocities)—exhibits more realistic scatter. Nevertheless, $\chi_\nu^2 < 1$ may indicate that: (i) reported uncertainties are somewhat conservative, (ii) positive correlations exist between measure-

ments sharing common calibration anchors, or (iii) there is a tendency for published results to cluster around previously established values.

The high precision of this combined estimate is driven by the recent JWST Cepheid measurements [3] and compatible results from other calibrators including TRGB [89], Miras [90], and SBF [125]. We note that the Lee et al. [87] JAGB measurement ($H_0 = 67.8 \pm 2.7$) represents a $\sim 2\sigma$ outlier within this category, as discussed in Section II.

2. Category 2: Local Λ CDM ($H_0 = 67.61 \pm 0.96 \text{ km s}^{-1} \text{Mpc}^{-1}$)

The 33 measurements in this category, which utilize local data but assume the Λ CDM expansion history, yield the *lowest* aggregate value of $H_0 = 67.61 \pm 0.96 \text{ km s}^{-1} \text{Mpc}^{-1}$. This value is fully consistent with, and in fact slightly lower than, the Planck CMB inference ($67.4 \pm 0.5 \text{ km s}^{-1} \text{Mpc}^{-1}$), despite being derived entirely from local observations.

The reduced chi-squared $\chi_\nu^2 = 0.80$ indicates internal consistency among these diverse methods (Strong Lensing, Gravitational Wave sirens, FRBs). This near-unity value suggests that the reported uncertainties accurately capture the true scatter and that no significant unrecognized systematics are present within this category.

In Figure 2, the distribution of category 2 appears at the lowest end of the parameter space, almost coincident with the Planck CMB value. This remarkable alignment between local Λ CDM-dependent measurements and early-universe physics—achieved without using the Sound Horizon—is one of the central findings of this work.

3. Category 3: Pure Local ($H_0 = 71.03 \pm 0.69 \text{ km s}^{-1} \text{Mpc}^{-1}$)

The 16 cosmological-model-independent measurements (Megamasers, Cosmic Chronometers, EPM) yield an intermediate value of $H_0 = 71.03 \pm 0.69 \text{ km s}^{-1} \text{Mpc}^{-1}$. Crucially, the removal of the Λ CDM shape assumption results in a central value shift of $\Delta H_0 = +3.42 \text{ km s}^{-1} \text{Mpc}^{-1}$ relative to Category 2. This shift is visible in Figure 2 as a broader distribution positioned between the Λ CDM-dependent results and the Distance Ladder.

The reduced chi-squared $\chi_\nu^2 = 0.77$ is lower than unity, indicating either conservative error estimates or the presence of correlations. This category exhibits significant internal heterogeneity: the Vogl et al. [112] tailored EPM measurement ($H_0 = 74.9 \pm 2.7$) strongly favors the Distance Ladder value, while most Cosmic Chronometer measurements favor values closer to Planck. This heterogeneity suggests that Category 3 may itself contain

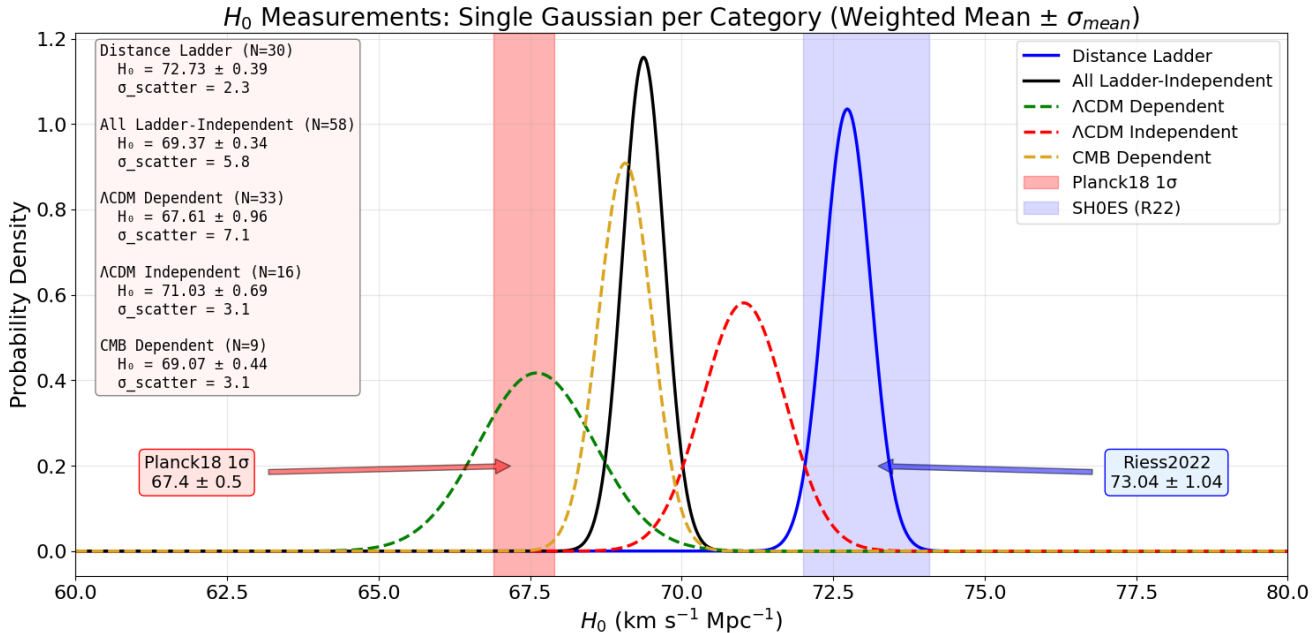


FIG. 2. **Gaussian probability distributions of the four measurement categories.** The visual separation is striking: Category 1 (Distance Ladder, blue peak) is isolated at high H_0 . Categories 2 (Local Λ CDM) and 4 (CMB-SHF) overlap significantly at low H_0 , demonstrating that local data analyzed under Λ CDM align with early-universe constraints. Category 3 (Pure Local) occupies a broader, intermediate region, highlighting the shift in central value when Λ CDM model assumptions are relaxed. The black curve represents the ensemble of all DLI-SHF measurements. The Planck 2018 value ($H_0 = 67.4 \pm 0.5 \text{ km s}^{-1} \text{ Mpc}^{-1}$) and SHOES value ($H_0 = 73.04 \pm 1.04 \text{ km s}^{-1} \text{ Mpc}^{-1}$) are indicated for reference.

distinct subpopulations, a possibility we explore further in Section IV.

4. Category 4: CMB Sound Horizon Free (CMB-SHF) ($H_0 = 69.07 \pm 0.44 \text{ km s}^{-1} \text{ Mpc}^{-1}$)

The 9 measurements utilizing CMB data without the Sound Horizon yield $H_0 = 69.07 \pm 0.44 \text{ km s}^{-1} \text{ Mpc}^{-1}$. This confirms that early-universe constraints on matter density (via the equality scale k_{eq}) favor a low H_0 regardless of the r_s calibration [118].

The reduced chi-squared $\chi^2_\nu = 0.89$ is very close to unity, indicating good internal consistency among the $N = 9$ measurements in this category. However, given that several measurements share common methodologies and partially overlapping datasets—particularly the Pogosian et al. [118, 121] and García Escudero et al. [122] results, which all employ Sound-Horizon-Free BAO analyses with DESI data—we examine potential correlations in Appendix C. In Figure 2, this distribution overlaps significantly with CMB-SHF measurements, reinforcing the consistency between early-universe physics and local data when Λ CDM is assumed.

C. Comparison: Distance Ladder vs. Combined Distance Ladder Independent/Sound Horizon Free (DLI-SHF)

To test the robustness of the “Early vs. Late” narrative, we combine all 58 DLI-SHF from Categories 2, 3, and 4 into a single ensemble. This combined sample represents the entirety of the evidence against the Distance Ladder that does not rely on the r_s standard ruler.

The weighted mean of this combined sample is:

$$H_0^{\text{All-Ladder-Indep}} = 69.37 \pm 0.34 \text{ km s}^{-1} \text{ Mpc}^{-1}. \quad (6)$$

This distribution is shown as the black curve in Figure 2 and the red curve in Figure 3, contrasting sharply with the Distance Ladder (blue curve). Figure 3 displays the probability density functions (PDFs) for the two measurement categories. Each individual measurement is represented as a Gaussian distribution, and the combined PDF is constructed as an inverse-variance weighted sum:

$$p_{\text{raw}}(H_0) = \sum_{i=1}^N w_i \cdot \mathcal{N}(H_0 | H_{0,i}, \sigma_i) \quad (7)$$

where $\mathcal{N}(x | \mu, \sigma)$ is the normal distribution:

$$\mathcal{N}(x | \mu, \sigma) = \frac{1}{\sigma \sqrt{2\pi}} \exp \left(-\frac{(x - \mu)^2}{2\sigma^2} \right) \quad (8)$$

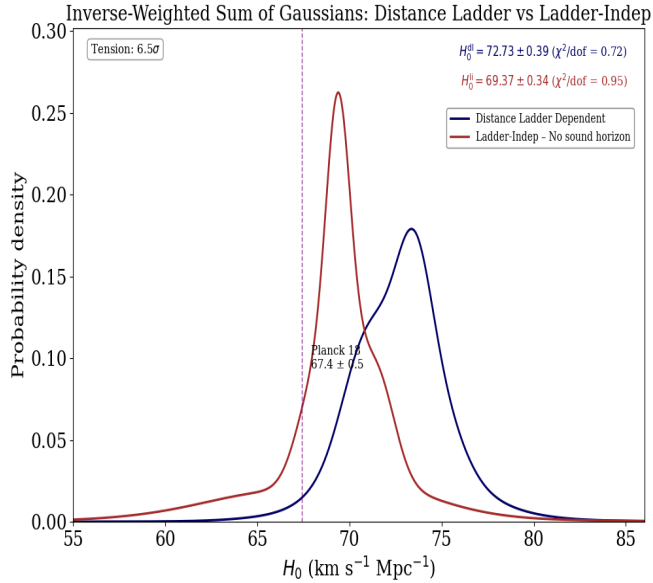


FIG. 3. The blue curve represents Category 1 (Distance Ladder, $H_0 = 72.73 \pm 0.39 \text{ km s}^{-1} \text{ Mpc}^{-1}$), while the red curve represents the combined ensemble of all DLI-SHF measurements (Categories 2+3+4, $H_0 = 69.37 \pm 0.34 \text{ km s}^{-1} \text{ Mpc}^{-1}$). The DLI-SHF curve is dominated by the CMB-SHF data which have the lowest uncertainty. The weighted mean tension between these two aggregate samples is 6.5σ (or 3.9σ after correlation adjustment). The vertical dashed line indicates the Planck 2018 value.

The final normalized PDF is obtained by dividing by the total area:

$$p(H_0) = \frac{p_{\text{raw}}(H_0)}{\int_{-\infty}^{\infty} p_{\text{raw}}(H'_0) dH'_0} \quad (9)$$

The two curves exhibit significant overlap despite the tension between their weighted means. This occurs because the image reflects the spread of individual measurement uncertainties σ_i (typically $2\text{--}10 \text{ km s}^{-1} \text{ Mpc}^{-1}$), whereas the uncertainty on the weighted mean is much smaller. Consequently, the PDF width is governed by the individual σ_i values, while the tension is calculated using the combined $\sigma_{\hat{H}_0}$ of Eq. (2).

This distinction explains why the curves overlap visually even when the weighted means differ by several standard deviations. The tension between the Distance Ladder and the Combined DLI-SHF sample is:

$$\Delta H_0 = 72.73 - 69.37 = 3.36 \text{ km s}^{-1} \text{ Mpc}^{-1}. \quad (10)$$

Combining the uncertainties in quadrature ($\sigma_{\text{diff}} = \sqrt{0.39^2 + 0.34^2} \approx 0.517 \text{ km s}^{-1} \text{ Mpc}^{-1}$), the significance of the discrepancy is:

$$n_{\sigma} = \frac{3.36}{0.517} \approx 6.5\sigma. \quad (11)$$

This 6.5σ tension exceeds the standard Planck vs. SH0ES discrepancy ($\sim 5\sigma$). It suggests that the Distance Ladder is in conflict not just with the CMB Sound Horizon, but with the aggregate of essentially all other cosmological probes that are independent of r_s .

1. Comparison with Previous Results

Table VII includes a comparison with our 2024 analysis [69]. Despite the significant expansion of the sample (from 53 to 88 measurements) and the refinement of the classification scheme (from 2 to 4 categories), the core results remain consistent:

- The Distance Ladder weighted mean has shifted slightly from 72.8 ± 0.5 to $72.73 \pm 0.39 \text{ km s}^{-1} \text{ Mpc}^{-1}$, with improved precision due to the inclusion of JWST measurements.
- The DLI-SHF weighted mean has shifted from 68.3 ± 0.5 to $69.37 \pm 0.34 \text{ km s}^{-1} \text{ Mpc}^{-1}$, remaining consistent within uncertainties.
- The tension has increased from $\sim 5\sigma$ to 6.5σ , primarily due to reduced uncertainties rather than a change in central values.

The stability of these results across independent analyses with different sample compositions strengthens confidence in the robustness of the “Distance Ladder vs. The Rest” characterization of the Hubble tension.

2. Impact of Correlations

The 6.5σ tension quoted above assumes statistical independence between measurements. As detailed in Appendix C, accounting for realistic correlations within each category increases the combined uncertainties. Using correlation coefficients estimated from shared calibration data and common methodology ($\bar{\rho} \approx 0.3\text{--}0.5$ for Distance Ladder; $\bar{\rho} \approx 0.1\text{--}0.2$ for DLI-SHF), we obtain:

$$H_0^{\text{Ladder,corr}} = 72.30 \pm 0.57 \text{ km s}^{-1} \text{ Mpc}^{-1}, \quad (12)$$

$$H_0^{\text{Ladder-Indep,corr}} = 69.52 \pm 0.42 \text{ km s}^{-1} \text{ Mpc}^{-1}. \quad (13)$$

The correlation-adjusted tension is:

$$n_{\sigma}^{\text{corr}} = \frac{72.30 - 69.52}{\sqrt{0.57^2 + 0.42^2}} \approx 3.9\sigma. \quad (14)$$

While reduced from 6.5σ , this tension remains highly significant and robust across the range of plausible correlation assumptions ($3.9\text{--}4.3\sigma$ for reasonable correlation models).

D. Internal Tension: Model Dependence

Beyond the external tension with the Distance Ladder, we identify a notable internal tension among the Distance Ladder Independent/Sound Horizon Free(DLI-SHF) measurements based on model assumptions. Comparing Category 2 (Local Λ CDM) with Category 3 (Pure Local), we find:

$$\Delta H_0^{\text{internal}} = 71.03 - 67.61 = 3.42 \text{ km s}^{-1} \text{ Mpc}^{-1}. \quad (15)$$

The statistical significance is:

$$n_{\sigma}^{\text{internal}} = \frac{3.42}{\sqrt{0.69^2 + 0.96^2}} \approx 2.9\sigma. \quad (16)$$

This 2.9σ internal tension, while not definitive, is suggestive of a systematic effect: imposing the Λ CDM model on local data appears to pull the inferred H_0 downward by $\sim 3.4 \text{ km s}^{-1} \text{ Mpc}^{-1}$. This shift accounts for more than half of the total Hubble tension ($\sim 6 \text{ km s}^{-1} \text{ Mpc}^{-1}$ between Distance Ladder and Planck).

We caution that this internal tension should be interpreted carefully for several reasons:

1. **Look-elsewhere effect:** We are comparing multiple categories, which increases the probability of finding a $\sim 2.9\sigma$ discrepancy by chance.
2. **Category heterogeneity:** As noted above, Category 3 contains measurements spanning a wide range of H_0 values (from ~ 66 to $\sim 75 \text{ km s}^{-1} \text{ Mpc}^{-1}$).
3. **Sample size:** Category 3 contains only 16 measurements, making the weighted mean sensitive to individual high-precision entries.

Nevertheless, the model-dependent shift is clearly observable in the offset between the Category 2 and Category 3 distributions in Figure 2, and its physical implications are explored further in Section IV.

E. Summary of Statistical Results

The key statistical findings of this section are:

1. The Distance Ladder yields $H_0 = 72.73 \pm 0.39 \text{ km s}^{-1} \text{ Mpc}^{-1}$, consistent with SH0ES and JWST measurements.
2. The combined DLI-SHF measurements yield $H_0 = 69.37 \pm 0.34 \text{ km s}^{-1} \text{ Mpc}^{-1}$, slightly elevated compared to our previous results but closer to Planck.
3. The tension between these two ensembles is 6.5σ (or 3.9σ after correlation adjustment).
4. Local measurements assuming Λ CDM (Category 2) yield systematically lower H_0 than cosmological-model-independent local measurements (Category 3), with a 2.9σ internal tension.

5. These results are consistent with, and strengthen, the conclusions of our 2024 analysis.

The implications of these findings—particularly the role of model assumptions and the apparent bimodality in the H_0 distribution—are explored in the following section.

IV. THE IMPACT OF MODEL ASSUMPTIONS

The results of Section III reveal a striking feature of the Hubble tension landscape: the discrepancy is not merely between the Distance Ladder and the Early Universe, but also manifests as an internal tension within the domain of Distance Ladder Independent/Sound Horizon Free (DLI-SHF) measurements. Specifically, the statistical compatibility of a measurement with the Planck value depends critically on whether the standard Λ CDM expansion history is assumed during the inference process. In this section, we dissect this model dependence, examine the critical role of specific high-precision measurements, and explore the physical implications of the observed bimodality in the H_0 distribution.

A. Implicit Bias of the Λ CDM Expansion History

The most significant finding of our four-category classification is the 2.9σ tension between local DLI-SHF measurements that assume a Λ CDM cosmology (Category 2: $H_0 = 67.61 \pm 0.96 \text{ km s}^{-1} \text{ Mpc}^{-1}$) and those that do not (Category 3: $H_0 = 71.03 \pm 0.69 \text{ km s}^{-1} \text{ Mpc}^{-1}$).

Measurements in Category 2, such as Gravitational Wave standard sirens [93] and standard analyses of Strong Lensing time delays [95], typically span the redshift range $0 < z < 1.5$. To extract H_0 from the observed luminosity distances or time delays, these methods must integrate the Hubble parameter $H(z)$:

$$d_L(z) = (1+z) \int_0^z \frac{cdz'}{H(z')}. \quad (17)$$

By fixing the functional form of $H(z)$ to that of flat Λ CDM (Eq. 1), often with Ω_m fixed to ≈ 0.3 or marginalized over a narrow prior, these analyses effectively impose a rigid shape constraint on the expansion history. The inferred H_0 is then the normalization that best fits the data given this assumed shape.

Our analysis shows that this Λ CDM shape constraint systematically prefers lower H_0 values ($H_0 \approx 67 \text{ km s}^{-1} \text{ Mpc}^{-1}$), aligning almost perfectly with the Planck CMB inference [1]. This demonstrates a remarkable self-consistency of the Λ CDM model: if one assumes the Λ CDM background evolution holds true at late times, local data (excluding the Distance Ladder) yields results consistent with early-universe physics, even without using the Sound Horizon [126].

However, when this shape constraint is released (Category 3), the inferred H_0 rises by $\Delta H_0 \approx +3.4 \text{ km s}^{-1} \text{ Mpc}^{-1}$ to $\approx 71 \text{ km s}^{-1} \text{ Mpc}^{-1}$. This shift has two possible interpretations:

1. **Λ CDM is correct, and Category 3 has larger systematics:** Cosmological-model-independent methods may suffer from unrecognized systematic errors that bias H_0 high. The lack of a shape constraint allows more freedom for systematics to propagate into the final result.
2. **The true $H(z)$ deviates from Λ CDM:** If the actual expansion history differs from the Λ CDM prediction at $z < 1$ (e.g., due to a late-time gravitational transition, dynamical dark energy, or modified gravity [69, 127–131]), forcing a Λ CDM fit would bias the inferred H_0 downward to compensate for the shape mismatch.

A related possibility is that the tension reflects not a global modification of $H(z)$, but rather a localized change in the physics governing distance calibrators. Refs [54–56, 58, 59] investigated whether a local variation in fundamental physics—such as a change in the fine-structure constant or gravitational strength within the calibration volume—could reconcile the SH0ES measurement with other probes without requiring modifications to the global expansion history. The current data do not definitively distinguish between these scenarios. A detailed comparison of late-transition versus smooth $H(z)$ deformation models has been presented in [132]. Earlier re-analyses of SH0ES data exploring additional degrees of freedom also found evidence for such model-dependent effects [133].

B. The Vogl et al. Tailored EPM: A Critical Test Case

Among the Category 3 measurements, the Vogl et al. [112] tailored Expanding Photosphere Method (EPM) result deserves particular attention. This measurement yields $H_0 = 74.9 \pm 2.7 \text{ km s}^{-1} \text{ Mpc}^{-1}$ (with systematic uncertainties — by the authors' own estimate comparable to the statistical errors — taken into account) is fully consistent with the Distance Ladder and in $\sim 2.9\sigma$ tension with the Planck value—yet it is completely independent of both the Distance Ladder calibration chain and cosmological model assumptions.

The EPM determines distances to Type II supernovae geometrically by combining measurements of the photospheric angular size (from flux and temperature) with the photospheric velocity (from spectral line Doppler shifts). The “tailored” approach of Vogl et al. advances this technique by using detailed non-local thermodynamic equilibrium (NLTE) radiative transfer models customized to individual supernovae, rather than the empirical dilution factors traditionally employed. This reduces model-

dependent systematics and achieves significantly smaller distance uncertainties.

The significance of this measurement for the Hubble tension debate is threefold:

1. **Independence from SNe Ia physics:** Unlike the Distance Ladder, which relies on the standardizability of SNe Ia, the tailored EPM uses SNe II—an entirely different supernova class with distinct explosion physics.
2. **Independence from calibrator physics:** The EPM does not require Cepheids, TRGB, or any other intermediate calibrator. It provides a direct geometric distance to the supernova.
3. **Independence from Λ CDM:** The method measures distances without integrating $H(z)$, making it insensitive to the assumed cosmological model.

If the Distance Ladder’s high H_0 were solely due to systematic errors in Cepheid photometry, metallicity corrections, or SNe Ia standardization, one would not expect an independent method like the tailored EPM to yield a consistent result. The agreement between Vogl et al. and the Distance Ladder suggests that either: (a) both methods share a common, as-yet-unidentified systematic, or (b) the high H_0 value reflects the true local expansion rate.

However, we note important caveats. The tailored EPM relies on assumptions about supernova explosion physics, ejecta composition, and atmospheric structure. The current sample is limited to a relatively small number of well-observed SNe II. Further validation with larger samples and independent atmosphere codes will be essential to confirm this result.

C. The Megamaser Perspective

A similar pattern emerges from Megamaser measurements. The Barua et al. [73] frequentist analysis of the Megamaser Cosmology Project (MCP) sample yields $H_0 = 73.5 \pm 3.0 \text{ km s}^{-1} \text{ Mpc}^{-1}$, again consistent with the Distance Ladder.

Megamaser distances are determined geometrically from the Keplerian dynamics of circumnuclear water maser disks, providing angular diameter distances that are in principle completely independent of stellar physics. However, Megamaser H_0 measurements are sensitive to the treatment of peculiar velocities, which become significant at the low redshifts ($z \lesssim 0.05$) where most masers hosts reside.

In our classification, we assigned the Barua et al [73] measurement to Category 2 because it relies primarily on Keplerian disk modeling without adopting Λ CDM-based peculiar velocity priors but relies on the Λ CDM prediction for the angular diameter distance. Indeed, when Ω_m is left as a free parameter rather than fixed to the Planck

value, the best-fit H_0 drops to $\sim 63 \text{ km s}^{-1} \text{ Mpc}^{-1}$ with uncertainties approximately five times larger, highlighting the model dependence of the headline result. In contrast, earlier analyses that adopted peculiar velocity corrections from the SH0ES flow model from Pesce et al. [134] would be more appropriately classified as having some distance ladder dependence.

The earlier Megamaser measurements by Kuo et al. [72] ($H_0 = 68 \pm 9 \text{ km s}^{-1} \text{ Mpc}^{-1}$) and Gao et al. [107] ($H_0 = 66 \pm 6 \text{ km s}^{-1} \text{ Mpc}^{-1}$) yielded lower values, though with larger uncertainties. The evolution toward higher H_0 in recent Megamaser analyses may reflect improved disk modeling, better peculiar velocity treatments, or statistical fluctuations in small samples.

D. Bimodality in the Distance Ladder Independent/Sound Horizon Free (DLI-SHF) Distribution

Although Figure 3 does not exhibit an obvious bimodal structure—the distribution of DLI-SHF measurements appears reasonably concentrated around a single peak—a more detailed examination reveals a subtle but significant effect.

To further explore the underlying structure of the DLI-SHF H_0 measurements, demonstrated also in figure 2, we employ a weighted Kernel Density Estimation (KDE) approach. Unlike a simple inverse-variance weighted sum of Gaussians, where each measurement contributes a Gaussian with width equal to its uncertainty σ_i , the KDE method assigns a fixed bandwidth h to all measurements while weighting their contributions according to their precision. The weighted KDE is defined as:

$$\hat{f}(x) = \sum_{i=1}^n w_i \cdot \frac{1}{\sqrt{2\pi}h} \exp\left(-\frac{(x-x_i)^2}{2h^2}\right), \quad (18)$$

where x_i is the measured H_0 value, h is the bandwidth (kernel width), and w_i are the normalized inverse-variance weights:

$$w_i = \frac{1/\sigma_i^2}{\sum_{j=1}^n 1/\sigma_j^2}. \quad (19)$$

This approach ensures that high-precision measurements contribute proportionally through their weights, but do not dominate the distribution through both weight *and* narrow kernel width simultaneously—a problem that arises with the standard inverse-variance weighted sum of Gaussians.

For this analysis, we exclude Category 4 measurements (CMB Sound Horizon Free), as these rely on CMB-derived data that provide exceptionally high precision. The three most precise Category 4 measurements—Pogosian et al. [118, 121] (DES: $69.37 \pm 0.65 \text{ km s}^{-1} \text{ Mpc}^{-1}$; pre-DES: $68.05 \pm 0.94 \text{ km s}^{-1} \text{ Mpc}^{-1}$) and Garcia et al. [122] (70.03 \pm

$0.97 \text{ km s}^{-1} \text{ Mpc}^{-1}$)—would alone account for approximately 65% of the total inverse-variance weight, clustering near $H_0 \approx 69 \text{ km s}^{-1} \text{ Mpc}^{-1}$ and obscuring any underlying structure in the remaining measurements.

The bandwidth h is a critical parameter controlling the smoothness of the KDE. Silverman's rule of thumb [135], which minimizes the mean integrated squared error assuming a unimodal Gaussian distribution, yields $h \approx 2.2 \text{ km s}^{-1} \text{ Mpc}^{-1}$ for our data. However, this criterion is known to oversmooth multimodal distributions. Given the *a priori* distinction between Category 2 (Λ CDM-dependent) and Category 3 (model-independent) measurements, a smaller bandwidth is justified to reveal potential substructure.

We find that bimodal structure is clearly visible for bandwidths in the range $h \in [1.1, 1.8] \text{ km s}^{-1} \text{ Mpc}^{-1}$. For $h < 1.1$, additional peaks emerge due to over-resolution of statistical fluctuations; for $h > 1.8$, the two peaks merge into a single mode with a shoulder. We adopt $h = 1.5 \text{ km s}^{-1} \text{ Mpc}^{-1}$, an intermediate value within the robust range, to balance resolution and smoothing.

The resulting distribution, shown in Figure 4, exhibits two distinct peaks corresponding to the weighted means of Category 2 ($\bar{H}_0 = 67.6 \text{ km s}^{-1} \text{ Mpc}^{-1}$) and Category 3 ($\bar{H}_0 = 71.0 \text{ km s}^{-1} \text{ Mpc}^{-1}$) measurements, with a separation of $\Delta H_0 = 3.4 \text{ km s}^{-1} \text{ Mpc}^{-1}$. This bimodal structure suggests a systematic difference between Λ CDM-dependent and cosmological-model-independent not Distance Ladder methods that warrants further investigation.

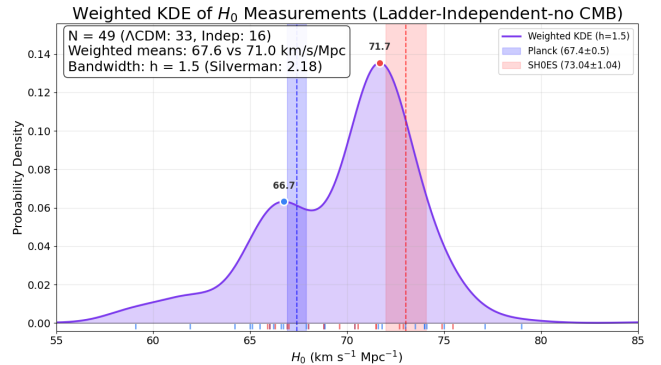


FIG. 4. Weighted Kernel Density Estimation (KDE) of DLI-SHF H_0 measurements, revealing the bimodal structure between Category 2 (Λ CDM-dependent) and Category 3 (model-independent) measurements. We adopt a bandwidth $h = 1.5 \text{ km s}^{-1} \text{ Mpc}^{-1}$, below the Silverman optimal value ($h \approx 2.2$), to prevent the distribution from being dominated by a few high-precision measurements. The bimodal structure remains robust across the range $h \in [1.1, 1.8]$; we select an intermediate value to balance resolution and smoothing. Weights are assigned as $w_i = 1/\sigma_i^2$, while the bandwidth is held constant across all measurements, ensuring that precise measurements contribute proportionally without overwhelming the distribution through both weight and kernel width.

E. Physical Interpretation of the Bimodality

If the bimodality is real and not an artifact of small-number statistics, it suggests that the “Hubble Tension” is not characterized by a single discrepant value but rather by a bifurcation of results based on methodology. The two peaks can be characterized as follows:

1. **The Low- H_0 Peak ($\sim 67 \text{ km s}^{-1} \text{ Mpc}^{-1}$):** Populated predominantly by:

- Category 2 measurements that assume ΛCDM (FRBs, GW sirens, most Strong Lensing)
- Cosmic Chronometer measurements in Category 3

These methods either explicitly assume ΛCDM or rely on physics that is ultimately calibrated by the same underlying cosmological model.

2. **The High- H_0 Peak ($\sim 73 \text{ km s}^{-1} \text{ Mpc}^{-1}$):** Populated by:

- Specific measurements: Megamasers [73] and tailored EPM [112]

These methods are characterized by their reliance on local geometric or kinematic physics.

This bifurcation pattern suggests a reformulation of the Hubble tension: the discrepancy may fundamentally be between *model-dependent* methods (which yield low H_0) and *local astrophysics dependent or cosmological-model-independent* methods (which yield high H_0), rather than between early and late times.

F. The Role of High-Precision Anchors

The tension landscape is significantly shaped by a small number of high-precision measurements that serve as “anchors” for the two solutions:

High- H_0 anchors:

- Riess et al. [3] JWST Cepheids: $H_0 = 73.49 \pm 0.93 \text{ km s}^{-1} \text{ Mpc}^{-1}$
- Zhang et al. [76] pairwise velocities: $H_0 = 75.5 \pm 3.8 \text{ km s}^{-1} \text{ Mpc}^{-1}$
- Vogl et al. [112] tailored EPM: $H_0 = 74.9 \pm 2.7 \text{ km s}^{-1} \text{ Mpc}^{-1}$

Low- H_0 anchors:

- Pogosian et al. [121] DESI BAO (no r_s): $H_0 = 69.37 \pm 0.65 \text{ km s}^{-1} \text{ Mpc}^{-1}$
- Kelly et al. [96] SN Refsdal: $H_0 = 66.6 \pm 3.7 \text{ km s}^{-1} \text{ Mpc}^{-1}$

Multi-parameter transition analyses of SH0ES data have explored how calibrator parameters may vary across the distance ladder, potentially contributing to the observed bifurcation. Evidence for possible transitions in Cepheid-SNe Ia calibrator parameters has been previously identified in the SH0ES sample [136, 137]. Recent work has also highlighted the subtle statistical effects in Distance Ladder analyses, including distance priors and selection effects, that could impact such comparisons [138]. The weighted means of each category are heavily influenced by these anchor measurements. Consequently, resolving the Hubble tension requires either: (a) identifying systematic errors in one or more anchor measurements, or (b) explaining why different methodologies yield systematically different results.

G. Category 3 as the Critical Adjudication Ground

The “Pure Local category (Category 3) serves as the critical test for distinguishing between the two interpretations of the Hubble tension. Currently, this category yields an intermediate value ($H_0 = 71.03 \pm 0.69 \text{ km s}^{-1} \text{ Mpc}^{-1}$), but it is internally heterogeneous:

- **High- H_0 subset:** Vogl EPM (74.9 ± 2.7), Palmese GW170817 (75.46 ± 5.4)
- **Low- H_0 subset:** Zhang CC+HII (65.9 ± 3.0), Li lensing (66.3 ± 3.7)

The future evolution of Category 3 will be decisive:

1. **If Category 3 converges toward Category 1 (ΛCDM):** This would strongly imply that the ΛCDM model assumption used in Category 2 is the source of the bias. Such convergence would suggest that the true late-time expansion history deviates from ΛCDM , requiring new physics (e.g., dynamical dark energy, modified gravity, or a late-time gravitational transition) such as the $\Lambda_s\text{CDM}$ model [139, 140]
2. **If Category 3 converges toward Category 2 (ΛCDM):** This would suggest that the Distance Ladder contains a unique, unrecognized systematic error affecting all its calibrators (Cepheids, TRGB, JAGB, Miras) in a similar way. Potential culprits include metallicity effects, dust extinction corrections, or environmental dependencies of SNe Ia.

Currently, the intermediate position of Category 3, combined with its internal heterogeneity, does not clearly favor either scenario. However, the existence of multiple independent cosmological-model-independent measurements (EPM, Megamasers) that support the high- H_0 solution is suggestive.

H. Summary: The Model-Dependence Effect

The key findings of this section can be summarized as follows:

1. Imposing Λ CDM assumptions on local kinematic data reduces the inferred H_0 by approximately $3.4 \text{ km s}^{-1} \text{ Mpc}^{-1}$ (from Category 3's 71.03 to Category 2's 67.61).
2. This shift accounts for more than half of the total Hubble tension ($\sim 6 \text{ km s}^{-1} \text{ Mpc}^{-1}$ between Distance Ladder and Planck).
3. The distribution shows evidence for bimodality with peaks corresponding to model-dependent (~ 67) and cosmological-model-independent (~ 73) methods.
4. Specific cosmological-model-independent measurements (Vogl EPM) yield high H_0 values consistent with the Distance Ladder, suggesting the high value may reflect true local physics rather than distance ladder systematics.
5. The future convergence or divergence of Category 3 measurements will be critical for determining whether the tension originates from Λ CDM model bias or distance ladder systematics.

These findings support a recharacterization of the Hubble tension as primarily a “Distance Ladder vs. The Rest” crisis, with a secondary “Model-Dependent vs. Cosmological-model-Independent” tension that may hold the key to its ultimate resolution.

V. DISCUSSION AND CONCLUSIONS

The “Hubble Tension” has long been framed as a cosmological crisis pitting the Early Universe (calibrated by the Sound Horizon) against the Late Universe (measured by the distance ladder). In this work, we have dissected this narrative by analyzing 88 measurements of H_0 that are strictly independent of the CMB Sound Horizon scale. Our findings suggest that the crisis is not necessarily a temporal one, but rather a methodological one. In this concluding section, we synthesize our results, discuss their implications for proposed solutions to the tension, and outline the observations needed to achieve resolution.

A. The “Distance Ladder vs. The Rest” Crisis

Our primary conclusion is that the Hubble tension is most accurately characterized as a discrepancy between the Distance Ladder methodology and essentially all other cosmological probes, regardless of whether those probes utilize early- or late-time data.

As detailed in Section III, the Distance Ladder (Category 1) yields a robust high value of $H_0 = 72.73 \pm 0.39 \text{ km s}^{-1} \text{ Mpc}^{-1}$. In stark contrast, when we combine all 58 independent measurements from Categories 2, 3, and 4—comprising Gravitational Waves, Strong Lensing, Cosmic Chronometers, Megamasers, FRBs, and Sound-Horizon-Free CMB data—we obtain a combined value of $H_0 = 69.37 \pm 0.34 \text{ km s}^{-1} \text{ Mpc}^{-1}$.

The resulting 6.5σ tension (3.9σ after correlation adjustment) between the Distance Ladder and the Distance Ladder Independent/Sound Horizon Free (DLI-SHF) ensemble exceeds the standard Planck vs. SH0ES discrepancy ($\sim 5\sigma$). This indicates that the high value of H_0 is a unique feature of the three-rung calibration chain (involving Cepheids/TRGB/Miras \rightarrow SNe Ia) and is not supported by the broader consensus of Sound-Horizon-Free cosmology.

This conclusion is robust across our analyses:

- It persists when correlations within categories are accounted for (Section III C).
- It is consistent with our 2024 analysis [69], despite the significant expansion of the sample.
- It holds regardless of which specific measurements are included or excluded (with the exception of complete removal of entire methodological classes).

B. Robustness of Results

To assess the sensitivity of our results to methodological choices in measurement categorization, we performed a comprehensive robustness analysis¹. We considered a more conservative approach to categorization by: (i) adopting alternative reported values for measurements with multiple H_0 estimates (Liu et al.: $59.1 \rightarrow 67.5 \text{ km s}^{-1} \text{ Mpc}^{-1}$; Dominguez et al.: $61.9 \rightarrow 65.6 \text{ km s}^{-1}$

TABLE VIII. Sensitivity analysis of tension estimates to categorization choices. The main tension between Distance Ladder and DLI-SHF methods remains highly significant ($> 5\sigma$) under all scenarios tested.

Scenario	Cat2 $H_0 \pm \sigma$	Cat3 $H_0 \pm \sigma$	Tension (DL-LI)	Tension (C2-C3)
Baseline (this work)	67.61 ± 0.96	71.03 ± 0.69	6.49σ	2.89σ
Liu: $59.1 \rightarrow 67.5$	68.27 ± 0.99	71.03 ± 0.69	6.22σ	2.29σ
Dominguez: $61.9 \rightarrow 65.6$	68.35 ± 1.01	71.03 ± 0.69	6.20σ	2.19σ
Remove Kelly (Refsdal)	67.68 ± 0.99	71.03 ± 0.69	6.35σ	2.78σ
Remove Li (Refsdal)	67.61 ± 0.96	71.19 ± 0.70	6.35σ	3.01σ
Remove Zhang 2022	67.61 ± 0.96	71.32 ± 0.71	6.32σ	3.11σ
Liu + Dominguez	69.15 ± 1.04	71.03 ± 0.69	6.01σ	1.51σ
All changes (keep Li)	69.37 ± 1.09	71.32 ± 0.71	5.86σ	1.50σ
All changes (keep Kelly)	69.15 ± 1.04	71.51 ± 0.72	5.86σ	1.87σ

¹ We thank Dan Scolnic for suggesting the examination of the categorization sensitivity for these specific cases to test the robustness of the internal tension.

Mpc^{-1}), (ii) removing potentially redundant measurements from the same observational data (Kelly/Li Refsdal analyses), and (iii) excluding measurements whose categorization could be debated (Zhang et al. 2022 cosmic chronometer analysis). Table VIII summarizes the impact of these changes on our tension estimates.

The analysis reveals that our main result—the significant tension between Distance Ladder and all others measurements—is robust to all tested variations in categorization methodology. Even under the most conservative scenario combining all alternative choices, the main tension remains at $\sim 5.9\sigma$, well above the 5σ threshold for statistical significance. No individual change affects the main tension by more than 0.29σ .

In contrast, the internal tension between Category 2 (ΛCDM -dependent) and Category 3 (cosmological-model-independent) measurements is more sensitive to these methodological choices, varying from 1.50σ to 3.11σ depending on the specific categorization adopted.

C. Implications for Proposed Solutions

Our findings have significant implications for the major classes of proposed solutions to the Hubble tension:

1. Early Dark Energy and Sound Horizon Modifications

Models that resolve the tension by reducing the Sound Horizon at recombination (e.g., Early Dark Energy [6, 40, 141], extra relativistic species, early modified gravity) predict that Sound-Horizon-Free measurements should align with the Distance Ladder. Our analysis shows the opposite: Distance Ladder Independent/Sound Horizon Free (DLI-SHF) (Categories 2, 3, and 4) yields a value closer to Planck, not to SH0ES.

This presents a significant challenge to early-universe solutions. If EDE or similar models were correct, we would expect:

- Megamaser distances to yield $H_0 \approx 73 \text{ km s}^{-1} \text{ Mpc}^{-1}$ ✓ (partially observed).
- GW standard sirens to yield $H_0 \approx 73 \text{ km s}^{-1} \text{ Mpc}^{-1}$ ✗ (observed: ≈ 68)
- Strong lensing to yield $H_0 \approx 73 \text{ km s}^{-1} \text{ Mpc}^{-1}$ ✗ (observed: $\approx 67\text{--}71$)
- Sound-Horizon-Free BAO to yield $H_0 \approx 73 \text{ km s}^{-1} \text{ Mpc}^{-1}$ ✗ (observed: ≈ 69)

The failure of most Sound-Horizon-Free probes to support the high- H_0 solution disfavors pure early-universe modifications as the complete explanation.

2. Late-Time Modifications

Models that modify the expansion history at late times (e.g., dynamical dark energy, late-time gravitational transitions, interacting dark energy) predict that the inferred H_0 should depend on whether ΛCDM is assumed in the analysis. Our observation of the Category 2 vs. Category 3 offset ($\Delta H_0 \approx 3.4 \text{ km s}^{-1} \text{ Mpc}^{-1}$) is qualitatively consistent with this prediction.

However, late-time solutions face their own challenges:

- They must explain why the shift is only $\sim 3 \text{ km s}^{-1} \text{ Mpc}^{-1}$, not the full $\sim 6 \text{ km s}^{-1} \text{ Mpc}^{-1}$ tension.
- They must be consistent with other late-time probes (SNe Ia Hubble diagrams, BAO, growth of structure) that show no dramatic deviation from ΛCDM .
- Recent DESI results [142–144] suggesting evolving dark energy ($w_0 > -1$, $w_a < 0$) provide evidence for deviations from ΛCDM at late times. However, due to the strong anti-correlation between w_0 and H_0 [145], such models with $w_0 > -1$ actually predict lower H_0 values, potentially exacerbating rather than alleviating the tension with the Distance Ladder. Moreover, the statistical significance of the DESI signal remains modest ($\sim 2\text{--}3\sigma$) and its robustness across different parameterizations has been questioned [146]. Theoretical frameworks for such behavior include models where the effective gravitational constant G_{eff} undergoes a rapid transition at late times, which can arise naturally in scalar-tensor theories. Recent re-examinations of such modified local physics scenarios using SH0ES data have refined the constraints on these models. A particularly intriguing perspective recasts the Hubble tension as an M crisis. Theodoropoulos & Perivolaropoulos demonstrated that if the intrinsic luminosity of SNe Ia in the Hubble flow differs systematically from that in calibrator galaxies, the inferred H_0 would be biased without requiring modifications to fundamental cosmology [54, 56, 147].

3. Distance Ladder Systematics

The isolation of the Distance Ladder as a 6.5σ outlier against 58 independent measurements points toward unrecognized systematics within the calibration chain. Potential systematic effects include:

- **Cepheid systematics:** Metallicity dependence of the period-luminosity relation, crowding and blending effects, or extinction corrections.
- **SNe Ia systematics:** Environmental dependencies (host galaxy mass, local star formation), evo-

lution with redshift, or standardization procedure biases [148–150].

- **Calibrator physics:** Differences between calibrators observed in anchor galaxies vs. SNe Ia hosts.
- **Sample selection:** Potential biases in which galaxies are selected for Cepheid observation.

However, the “systematics” interpretation faces its own challenges:

- Multiple independent calibrators (Cepheids, TRGB, JAGB, Miras, SBF) yield consistent high- H_0 values.
- JWST observations have largely confirmed HST Cepheid photometry [3].
- Cosmological-model-independent methods like the tailored EPM [112] support the high- H_0 solution.

4. Hybrid Scenarios

Given the complexity of the evidence, a hybrid scenario involving *both* partial distance ladder systematics *and* deviations from Λ CDM dynamics may be required. For example:

- A $\sim 2\%$ systematic in the distance ladder calibration (reducing its H_0 by $\sim 1.5 \text{ km s}^{-1} \text{ Mpc}^{-1}$)
- Combined with a late-time modification to $H(z)$ (accounting for the remaining $\sim 1.5\text{--}3 \text{ km s}^{-1} \text{ Mpc}^{-1}$)

Such a scenario is constrained but not excluded by current data.

D. Falsifiability and Future Tests

A robust scientific framework requires clear predictions that can be tested by future observations. We outline the key tests that would distinguish between the competing interpretations:

1. What Would Confirm Distance Ladder Systematics?

The “systematics” hypothesis would be strongly supported if:

1. Category 3 measurements converge toward $H_0 \approx 67 \text{ km s}^{-1} \text{ Mpc}^{-1}$ as precision improves.
2. Future Megamaser measurements yield $H_0 < 70 \text{ km s}^{-1} \text{ Mpc}^{-1}$ with reduced uncertainties.
3. The tailored EPM, applied to larger SNe II samples, yields $H_0 < 70 \text{ km s}^{-1} \text{ Mpc}^{-1}$.

4. A specific systematic is identified in the distance ladder (e.g., a metallicity correction error) that shifts its H_0 down by $\sim 5 \text{ km s}^{-1} \text{ Mpc}^{-1}$.
5. Independent geometric distance methods (e.g., detached eclipsing binaries in external galaxies) yield distances inconsistent with Cepheids.

2. What Would Confirm New Physics?

The “new physics” hypothesis would be strongly supported if:

1. Category 3 measurements converge toward $H_0 \approx 73 \text{ km s}^{-1} \text{ Mpc}^{-1}$ as precision improves.
2. Multiple independent cosmological-model-independent methods (EPM, Megamasers, future techniques) consistently yield $H_0 > 72 \text{ km s}^{-1} \text{ Mpc}^{-1}$.
3. GW standard sirens, analyzed without assuming Λ CDM (e.g., using cosmographic methods), yield higher H_0 than Λ CDM-based analyses.
4. Direct evidence for deviations from Λ CDM at $z < 1$ emerges from other probes (e.g., DESI dark energy constraints, growth rate measurements).
5. A theoretical model is developed that simultaneously explains the Hubble tension, the Category 2 vs. Category 3 offset, and passes all other cosmological tests.

E. Observational Priorities

Based on our analysis, we identify the following observational priorities for resolving the Hubble tension:

1. **Expand Category 3 (Pure Local):** This category currently contains only 16 measurements with significant internal heterogeneity. Additional cosmological-model-independent measurements are crucial for determining whether the intermediate $H_0 \approx 70 \text{ km s}^{-1} \text{ Mpc}^{-1}$ persists or converges toward one of the two solutions.
2. **Improve tailored EPM precision:** The Vogl et al. [112] result is currently the strongest cosmological-model-independent support for the high- H_0 solution outside the traditional Distance Ladder. Larger SNe II samples observed with JWST spectroscopy could significantly reduce uncertainties.
3. **Expand Megamaser sample:** Additional Megamaser host galaxies at $z > 0.05$ (where peculiar velocities are subdominant) would provide crucial geometric distance constraints.

4. **Accumulate GW standard sirens:** The LIGO-Virgo-KAGRA O4 and O5 [151] runs will significantly increase the sample of both bright and dark sirens. Crucially, these should be analyzed both with and without Λ CDM assumptions to test for model-dependent biases.
5. **Cosmological-model-independent Strong Lensing:** Future time-delay measurements should emphasize cosmographic or cosmological-model-independent analyses alongside standard Λ CDM fits.
6. **Cross-calibration tests:** Direct comparisons between different calibrators (Cepheids vs. TRGB vs. JAGB) in the same galaxies can identify potential systematics.

F. Concluding Remarks

The Hubble tension remains one of the most significant challenges to the standard cosmological model. Our analysis of 88 Sound-Horizon-Free measurements reveals that the tension is more accurately characterized as a “Distance Ladder vs. The Rest” crisis rather than an “Early vs. Late Universe” discrepancy.

The key findings of this work are:

1. The Distance Ladder yields $H_0 = 72.73 \pm 0.39 \text{ km s}^{-1} \text{ Mpc}^{-1}$, while all other Distance Ladder Independent/Sound Horizon Free(DLI-SHF) methods combined yield $H_0 = 69.37 \pm 0.34 \text{ km s}^{-1} \text{ Mpc}^{-1}$, a 6.5σ (3.9σ correlation-adjusted) tension.
2. Local measurements do not universally favor high H_0 . When analyzed under Λ CDM assumptions, local probes yield values consistent with Planck.
3. A 2.9σ internal tension exists between Λ CDM-dependent (Category 2) and cosmological-model-independent (Category 3) local measurements, with the Λ CDM assumption reducing inferred H_0 by $\sim 3.4 \text{ km s}^{-1} \text{ Mpc}^{-1}$.
4. Specific cosmological-model-independent measurements (e.g., tailored EPM) support the high- H_0 solution, complicating the pure “systematics” interpretation.
5. The evidence disfavors pure early-universe solutions (like Early Dark Energy) but does not definitively confirm either late-time modifications or Distance Ladder systematics.

The resolution of the Hubble tension will likely require a combination of improved observations, careful systematic analysis, and potentially a revision of our understanding of either astrophysical calibrators or fundamental cosmology. The four-category classification scheme

introduced in this work provides a framework for tracking progress toward this resolution as new measurements become available.

Whatever the ultimate explanation, the Hubble tension has already achieved a valuable scientific outcome: it has motivated an unprecedented scrutiny of both our measurement techniques and our theoretical assumptions, pushing cosmology toward greater rigor and potentially toward new discoveries. Recent results from the Atacama Cosmology Telescope DR6 provide additional CMB constraints that will be crucial for further testing the robustness of our conclusions [152, 153].

ACKNOWLEDGMENTS

This research was supported by COST Action CA21136 – Addressing observational tensions in cosmology with systematics and fundamental physics (CosmoVerse), supported by COST (European Cooperation in Science and Technology). We thank Adam Riess and Dan Scolnic for their detailed and constructive comments on measurement categorization, which helped us strengthen and clarify our analysis. We are grateful to Levon Pogosian for providing the unpublished DESI DR2 Sound-Horizon-Free result and to Helena García Escudero and Seyed Hamidreza Mirpoorian for sharing their work prior to publication. We thank Pilar Ruiz-Lapuente for useful correspondence regarding the JAGB calibration debate and for providing her “SNe Ia twins” measurement prior to its inclusion in our compilation. We also thank Yi-Ying Wang for pointing out relevant FRB and gravitational wave measurements, and Yi-min Zhang for sharing results on interacting dark energy models.

Appendix A: Complete Data Tables

In this appendix, we provide expanded versions of the data tables presented in the main text, including additional metadata and methodological details for each measurement. These tables serve as a comprehensive reference for future analyses and allow readers to assess the classification of individual measurements.

TABLE IX. Detailed statistical summary for each measurement category.

Category	N	$\langle H_0 \rangle$	σ	χ^2_ν	Range
1. Distance Ladder	30	72.73	0.39	0.72	67.8–77.0
2. Local (Λ CDM)	33	67.61	0.96	0.80	54.6–86.2
3. Pure Local	16	71.03	0.69	0.77	65.9–75.5
4. CMB-SHF	9	69.07	0.44	0.89	61–70.8
Combined DLI-SHF (2+3+4)	58	69.37	0.34	0.95	54.6–86.2

Notes: $\langle H_0 \rangle$ is the inverse-variance weighted mean in $\text{km s}^{-1} \text{ Mpc}^{-1}$. Range shows min–max of central values.

1. Distance Ladder Measurements: Extended Information

Table X provides extended information for all 30 Distance-Ladder-dependent H_0 measurements. We include the geometric anchor(s) employed, the primary distance indicator, the secondary distance indicator (if applicable), and the reported H_0 value with uncertainty.

The measurements span a range of calibrator types:

- **Cepheids:** 11 measurements, anchored primarily to NGC 4258, LMC, and MW parallaxes
- **TRGB:** 7 measurements, typically anchored to LMC detached eclipsing binaries
- **JAGB:** 2 measurements with notably discrepant results (Li vs. Lee)
- **Mira variables:** 3 measurements
- **SBF/Tully-Fisher:** 5 measurements using secondary calibration
- **Other:** 2 measurements (pairwise velocities, HII regions)

2. Distance Ladder Independent/Sound Horizon Free (DLI–SHF) Measurements: Extended Information

Table XI provides extended information for all 58 DLI–SHF H_0 measurements from Categories 2, 3, and 4. We include the physical observable, the cosmological probe, the model assumptions (which determine the category assignment), and the reported H_0 value with uncertainty.

The “Model” column indicates the category assignment:

- **Λ CDM:** Category 2 — Analysis explicitly assumes flat Λ CDM expansion history
- **Independent:** Category 3 — Cosmological model-independent analysis (geometric, cosmographic, or direct $H(z)$)
- **CMB–NSH:** Category 4 — Uses CMB data but avoids Sound Horizon (No Sound Horizon)

The measurements span diverse physical probes:

- **Strong Gravitational Lensing:** 18 measurements (time delays from quasars, SNe, and clusters)
- **Gravitational Waves:** 9 measurements (bright and dark sirens)
- **Fast Radio Bursts:** 7 measurements (dispersion measure–redshift relation)

- **Cosmic Chronometers:** 4 measurements (differential galaxy ages)
- **Megamasers:** 3 measurements (geometric disk distances)
- **CMB-based (no r_s):** 9 measurements (SZ effect, k_{eq} scale, etc.)
- **Other:** 8 measurements (EPM, kilonovae, gamma-ray attenuation, etc.)

3. Statistical Summary by Category

Table IX provides a detailed statistical breakdown of each category, including the number of measurements, weighted mean, standard error, reduced chi-squared, and the range of individual measurements.

Appendix B: Individual Measurement Descriptions

In this appendix, we provide detailed descriptions of selected measurements that are particularly important for understanding the Hubble tension landscape. We focus on measurements that either anchor the tension (high-precision results), represent methodological innovations, or exhibit notable discrepancies with other measurements in their class.

1. Key Distance Ladder Measurements

a. Riess *et al.* (2022, 2025): The SH0ES Program

The SH0ES (Supernova H_0 for the Equation of State) collaboration has produced the most precise Distance-Ladder measurements of H_0 . The methodology employs a three-rung distance ladder:

Rung 1 (Geometric Anchors): Three independent anchors establish the absolute distance scale:

- Gaia EDR3 parallaxes to Milky Way Cepheids (corrected for zero-point offset)
- Megamaser geometric distance to NGC 4258 [189]
- Detached eclipsing binary distances to the LMC [190]

Rung 2 (Cepheid Calibration): Cepheid variables observed with HST WFC3 in the F160W (H-band) filter provide period–luminosity relations in 37+ galaxies hosting Type Ia supernovae. The use of Wesenheit magnitudes, $m_H^W = m_H - R(m_V - m_I)$, eliminates reddening dependence by construction.

Rung 3 (Hubble Flow SNe Ia): The calibrated SNe Ia absolute magnitude M_B is applied to the Pantheon+ sample in the redshift range $0.023 < z < 0.15$.

TABLE X. Extended information for all 30* Distance-Ladder H_0 measurements (Category 1). Columns show the measurement index, author/year with citation, H_0 value ($\text{km s}^{-1} \text{Mpc}^{-1}$), geometric anchor(s), primary distance indicator, secondary indicator, and redshift range. Measurements are ordered chronologically.

#	Author (Year)	$H_0 \pm \sigma$	Anchor	Primary	Secondary	z range
1	Huang (2019) [80]	73.3 \pm 4.0	NGC 4258, MW, LMC	Mira	SNe Ia	< 0.15
2	de Jaeger (2020) [81]	75.8 \pm 5.1	LMC, MW	Cepheids/TRGB	SNe II	< 0.1
3	Kourkchi (2020) [154]	76.0 \pm 2.5	Cepheids, TRGB	Tully–Fisher	—	< 0.05
4	Khetan (2021) [82]	70.50 \pm 4.13	Cepheids, TRGB	SBF	SNe Ia	< 0.075
5	Blakeslee (2021) [125]	73.3 \pm 2.5	NGC 4258, LMC	SBF	SNe Ia	< 0.08
6	Freedman (2021) [83]	69.8 \pm 1.7	LMC (DEB), MW	TRGB	SNe Ia	< 0.08
7	Dhawan (2022) [155]	76.94 \pm 6.4	LMC	TRGB	SNe Ia	< 0.08
8	Kenworthy (2022) [84]	73.1 \pm 2.5	NGC 4258, LMC	Cepheids	—	< 0.1
9	Dhawan (2022) [156]	70.92 \pm 1.88	LMC	TRGB	SNe Ia	< 0.08
10	Dhawan (2022) [156]	74.82 \pm 1.28	NGC 4258, LMC, MW	Cepheids	SNe Ia	< 0.15
11	Scolnic (2023) [85]	73.22 \pm 2.06	LMC	TRGB	SNe Ia	< 0.15
12	de Jaeger (2023) [157]	74.1 \pm 8.0	LMC, MW	Cepheids	SNe II	< 0.1
13	Uddin (2023) [158]	71.76 \pm 1.32	Multiple	Combined	SNe Ia	< 0.1
14	Uddin (2023) [158]	73.22 \pm 1.45	Multiple	Combined	SNe Ia	< 0.1
15	Huang (2023) [159]	72.37 \pm 2.97	NGC 4258, LMC	Mira	SNe Ia	< 0.15
16	Li (2024) [86]	74.7 \pm 3.1	LMC, SMC	JAGB	SNe Ia	< 0.08
17	Chavez (2024) [160]	73.1 \pm 2.3	Cepheids	H II L – σ	—	< 0.2
18	Boubel (2024) [161]	73.3 \pm 4.1	Cepheids, TRGB	Tully–Fisher	—	< 0.05
19	Lee (2024) [87]	67.80 \pm 2.72	LMC	JAGB	SNe Ia	< 0.08
20	Freedman (2024) [75]	72.05 \pm 3.60	LMC (DEB), MW	Cepheids	SNe Ia	< 0.08
21	Said (2024) [162]	76.05 \pm 4.90	SBF	Fund. Plane	—	< 0.1
22	Zhang (2024) ^a [76]	75.5 \pm 3.8	—	Pairwise Vel.	—	< 0.1
23	Jensen (2025) [89]	73.8 \pm 2.4	LMC, MW	TRGB	—	< 0.03
24	Wojtak (2025) [163]	70.59 \pm 1.15	NGC 4258, LMC, MW	Cepheids	SNe Ia	< 0.15
25	Bhardwaj (2025) [90]	73.06 \pm 2.6	NGC 4258, LMC	Mira	SNe Ia	< 0.15
26	Newman (2025) [91]	75.3 \pm 2.9	LMC	TRGB	SNe Ia	< 0.08
27	Riess (2025) ^b [3]	73.49 \pm 0.93	NGC 4258, LMC, MW	Cepheids	SNe Ia	< 0.15
28	Kudritzki (2025) [164]	76.2 \pm 6.2	FGLR	Tully–Fisher	—	< 0.05
29	Wagner (2025) ^c [165]	68 \pm 8	—	TRGB	Infall	< 0.02
30	Lapuente (2025) [88]	72.61 \pm 1.69	—	M 101, NGC 5643, NGC 7250, M 66	SNe Ia (twins)	< 0.09

Notes: DEB = Detached Eclipsing Binaries; FGLR = Flux-weighted Gravity–Luminosity Relation; SBF = Surface Brightness Fluctuations. Entries #19 (Lee 2024) and #29 (Wagner 2025) are notable low- H_0 outliers within this category.

^a Includes systematic uncertainties not fully accounted for in the original analysis; see Appendix B.

^b We adopt this measurement for all numerical H_0 values in this work. For comparisons, we use the SH0ES 2022 result [2] as reference baseline, given its established presence in the literature.

^c Assumes a local expansion parameter $\kappa = 1.4$ with no uncertainties. We adopt $\kappa = 1.3 \pm 0.1$ in our analysis; see Appendix B.

The 2022 HST result [2] yielded $H_0 = 73.04 \pm 1.04 \text{ km s}^{-1} \text{Mpc}^{-1}$ (1.4% precision). The 2025 JWST result [3] yields $H_0 = 73.49 \pm 0.93 \text{ km s}^{-1} \text{Mpc}^{-1}$ (1.3% precision), confirming the HST photometry and ruling out crowding-induced biases as the source of the tension.

Systematic Error Budget: The SH0ES analyses include comprehensive systematic assessments for Cepheid photometry ($\sim 0.5 \text{ km s}^{-1} \text{Mpc}^{-1}$), metallicity effects ($\sim 0.4 \text{ km s}^{-1} \text{Mpc}^{-1}$), crowding corrections ($\sim 0.3 \text{ km s}^{-1} \text{Mpc}^{-1}$), SNe Ia standardization ($\sim 0.5 \text{ km s}^{-1} \text{Mpc}^{-1}$), and peculiar velocities ($\sim 0.3 \text{ km s}^{-1} \text{Mpc}^{-1}$).

b. Freedman *et al.* (2021, 2024): The CCHP TRGB Program

The Chicago-Carnegie Hubble Program (CCHP) developed the Tip of the Red Giant Branch (TRGB) as an

alternative to Cepheids. The TRGB method exploits the helium flash that terminates red giant branch evolution at a nearly constant luminosity ($M_I \approx -4.05$), producing a sharp discontinuity detectable via edge-detection algorithms (Sobel filter).

The 2021 analysis [83] yielded $H_0 = 69.8 \pm 1.7 \text{ km s}^{-1} \text{Mpc}^{-1}$, intermediate between Planck and SH0ES. This sparked debate about whether TRGB measurements genuinely favor lower H_0 or whether methodological differences explain the offset from SH0ES.

The 2024 JWST analysis [75] found $H_0 = 72.05 \pm 3.60 \text{ km s}^{-1} \text{Mpc}^{-1}$ from Cepheids, now more consistent with SH0ES. The CCHP continues to analyze TRGB and JAGB calibrations from JWST data.

TABLE XI. Extended information for all 58 DLI–SHF H_0 measurements (Categories 2, 3, and 4). Columns show the measurement index, category assignment, author/year with citation, H_0 value ($\text{km s}^{-1} \text{Mpc}^{-1}$), primary observable, cosmological probe, and model assumptions. Measurements are ordered by category, then chronologically within each category.

#	Cat.	Author (Year)	$H_0 \pm \sigma$	Observable	Probe	Model	z range
Category 2: Local (ΛCDM Assumption) — 33 measurements							
1	2	Wu (2021) [98]	$68.81^{+4.99}_{-4.33}$	Dispersion measure, z	FRBs	Λ CDM	0.0039–0.695
2	2	Abbott (2021) [93]	68^{+8}_{-6}	GW strain amplitude	CBC dark sirens	Λ CDM	< 0.5
3	2	Shajib (2023) [95]	$77.1^{+7.3}_{-7.1}$	Time delays, dynamics	Lensed quasars	Λ CDM	0.657
4	2	Napier (2023) [100]	74.1 ± 8.0	Time delays	Cluster lenses	Λ CDM	1.734–2.805
5	2	Kelly (2023) [96]	$66.6^{+4.1}_{-3.3}$	Time delays	SN Refsdal	Λ CDM	1.49
6	2	Dominguez (2023) [166]	$61.9^{+2.9}_{-2.4}$	γ -ray opacity	Blazar spectra	Λ CDM †	< 6
7	2	Gao (2023) [167]	$65.5^{+6.4}_{-5.4}$	DM– z + SNe Ia	FRBs	Λ CDM	0.039–2.3
8	2	Liu (2023) [101]	$59.1^{+6.6}_{-3.5}$	Time delays	Cluster lensed QSO	Λ CDM	< 3.33
9	2	Fung (2023) [168]	86^{+55}_{-46}	GW strain only	NSBH population	Λ CDM	< 0.25
10	2	Martinez (2023) [102]	74^{+9}_{-13}	Time delays	Lensed quasars	Λ CDM	1.734
11	2	Ballard (2023) [169]	$85.4^{+29.1}_{-33.9}$	GW strain + galaxy z	Dark siren	Λ CDM	< 0.5
12	2	Moresco (2023) [108]	66.7 ± 5.3	Spectroscopic ages	Passive galaxies	Λ CDM	0.07–1.965
13	2	Alfradique (2024) [170]	$68.84^{+15.51}_{-7.74}$	GW strain + galaxy z	Dark sirens	Λ CDM	< 0.1
14	2	Grillo (2024) [171]	$66.2^{+3.5}_{-2.2}$	Time delays	HFF clusters	Λ CDM	1.240–3.703
15	2	Pascale (2024) [103]	$71.8^{+9.2}_{-8.1}$	Time delays	Hope SN (JWST)	Λ CDM	1.78
16	2	Hernandez (2024) [172]	$73.0^{+13.7}_{-7.7}$	GW + BGP	Spectral sirens	Λ CDM	< 1.5
17	2	Bom (2024) [173]	$70.4^{+13.6}_{-11.7}$	GW + kilonova	O4a events	Λ CDM	0.1–0.6
18	2	TDCOSMO XVI (2024) [174]	65^{+23}_{-14}	Time delays	WGD2038	Λ CDM	0.777
19	2	Gao (2024) [175]	68.81 ± 5.64	DM– z relation	Localized FRBs	Λ CDM	0.0008–1.016
20	2	Li (2024) [176]	66 ± 5	Time delays (corrected)	Lensed quasars	Λ CDM	< 2.5
21	2	Yang (2024) [104]	$74.0^{+7.5}_{-7.2}$	DM + scattering	FRBs	Λ CDM	0.034–1.016
22	2	Piratova-Moreno (2025) ‡ [99]	65.1 ± 7.4	DM– z relation	FRBs (MLE)	Λ CDM	0.0008–1.354
23	2	Barua (2025) [73]	$73.5^{+3}_{-2.9}$	Maser dynamics	MCP sample	Λ CDM	0.002–0.034
24	2	Zhang (2025) [177]	75 ± 30	PRS association	FRBs	Λ CDM	0.03–0.25
25	2	Gao (2025) [178]	$86.18^{+18.03}_{-14.99}$	RM–PRS correlation	FRBs	Λ CDM	0.098–0.241
26	2	Loubser (2025) [179]	54.6 ± 26.3	Spectroscopic ages	BCGs	Λ CDM	0.3–0.7
27	2	Beirnaert (2025) [94]	79 ± 9	GW strain	Dark sirens (avg)	Λ CDM	< 1
28	2	Bahr-Kalus (2025) [117]	$74.0^{+7.2}_{-3.5}$	Turnover scale + BAO	DESI	Λ CDM	0.4–3.1
29	2	Birrer (2025) [97]	$71.6^{+3.9}_{-3.3}$	Time delays + kinematics	Multiple lenses	Λ CDM	0.082–0.745
30	2	Liu (2025) [180]	66.0 ± 4.3	Strong grav. lensing	Multiple lenses	Λ CDM	1.49
31	2	Pierel (2025) [105]	$66.6^{+11.2}_{-8.1}$	Time delays	SN Encore	Λ CDM	1.95
32	2	Paic (2025) [181]	$64.2^{+5.8}_{-5}$	Strong Lensing	SMARTS	Λ CDM	2.32
33	2	Oliveira (2026) [182]	$67.9^{+4.4}_{-4.3}$	3 \times 2pt + Standard Sirens	Shear/positions + GW strain	Λ CDM	0.1–2
Category 3: Pure Local (Cosmological-Model Independent) — 16 measurements							
34	3	Kuo (2013) [72]	68 ± 9	Maser positions, velocities	Megamaser disk	Independent	0.034
35	3	Gao (2015) [107]	66 ± 6	Maser positions, velocities	Megamaser disk	Independent	0.028
36	3	Bulla (2022) [183]	69.6 ± 5.5	GW + kilonova light curve	BNS merger	Independent	0.01
37	3	Zhang (2022) [109]	65.9 ± 3.0	Spectroscopic ages	Passive galaxies	Independent	0.009–2.545
38	3	Du (2023) [110]	$71.5^{+4.4}_{-3}$	Time delays + GRBs	Lensed quasars	Independent	0.654–2.375
39	3	Palmessi (2023) [92]	$75.46^{+5.34}_{-5.39}$	GW + afterglow	GW170817	Independent	0.01
40	3	Sneepen (2023) [111]	67.0 ± 3.6	Photospheric velocity	Kilonova	Independent	0.0986
41	3	Liu (2023) [184]	$72.9^{+2.0}_{-2.3}$	Lensing + SNe Ia	Combined	Independent	0.01–2.3
42	3	Gonzalez (2024) [185]	$72.7^{+6.3}_{-5.6}$	Gas fraction + SNe Ia	Clusters	Independent	0.01–2.3
43	3	Li (2024) [113]	$66.3^{+3.8}_{-3.6}$	Time delays	SN Refsdal	Independent	0.001–2.261
44	3	Jaiswal (2024) [186]	$66.9^{+10.6}_{-2.1}$	RM lag	NGC 5548	Independent	0.017
45	3	Vogl (2024) [112]	74.9 ± 2.7	Photospheric expansion	SNe II	Independent	0.01–0.04
46	3	Song (2025) [114]	$70.40^{+8.03}_{-5.60}$	GW + lensing	Combined	Independent	< 0.8
47	3	Colaco (2025) [187]	70.55 ± 7.44	Lensing + SNe Ia	Joint	Independent	0.001–2.261
48	3	Du (2025) [188]	71.59 ± 0.94	CC+BAO+ SNe Ia	IDL+ MAPAge	Independent	0.001–2.5
49	3	Favale (2025) [115]	68.8 ± 3.0	Ages + SNe Ia	CC + Pantheon+	Independent	0.07–1.965
Category 4: CMB Sound Horizon Free (CMB–SHF) — 9 measurements							
50	4	Reese (2003) [119]	61 ± 18	SZ decrement, X-ray	Galaxy clusters	CMB–NSH	0.02–0.83
51	4	Philcox (2022) [116]	$64.8^{+2.2}_{-2.5}$	BAO scale, shape	Matter–rad. eq.	CMB–NSH	0.2–0.75
52	4	Colaco (2023) [120]	67.22 ± 6.07	SZ + X-ray + SNe Ia	Clusters	CMB–NSH	0.01–2.3
53	4	Pogosian (2024) [118]	68.05 ± 0.94	BAO peak + BBN	Pre-DESI BAO	CMB–NSH	0.1–4.16
54	4	Pogosian (2025) [121]	69.37 ± 0.65	BAO peak + BBN	DESI DR BAO	CMB–NSH	0.1–4.16
55	4	Bahr-Kalus (2025) [117]	$65.4^{+4.9}_{-6.2}$	Turnover scale + SNe	DESI + Pantheon+	CMB–NSH	0.4–3.1
56	4	Garcia (2025) [122]	70.03 ± 0.97	BAO+ θ^* + CMB lensing	DESI+APSF+ DES 3 \times 2pt	CMB–NSH	0.1–4.2
57	4	Zaborowski (2023) [123]	$70.8^{+2.0}_{-2.2}$	BAO+ θ^*	Clust.+ BAO+ Lym.- α	CMB–NSH	0.1–4.2
58	4	Krolewski (2025) [124]	69.0 ± 2.5	DESI DR1 + CMB	Energy densities	CMB–NSH	0.1–2.33

Notes: CMB–NSH = CMB-based, No Sound Horizon; MLE = Maximum Likelihood Estimator; PRS = Persistent Radio Source; RM = Reverberation Mapping; BGP = Binary Gravitational-wave Population; HFF = Hubble Frontier Fields; BNS = Binary Neutron Star; NSBH = Neutron Star–Black Hole.

† $\Omega_m = 0.3$ fixed.

‡ Includes systematic uncertainties not fully accounted for in the original analysis; see Appendix B.

c. *Lee et al. (2024): The Low- H_0 JAGB Outlier*

The Lee et al. [87] JAGB analysis yields $H_0 = 67.8 \pm 2.7 \text{ km s}^{-1} \text{ Mpc}^{-1}$, consistent with Planck and $\sim 2\sigma$ below other Distance Ladder measurements. This represents the most significant outlier within Category 1.

The JAGB method uses carbon stars on the Asymptotic Giant Branch, which exhibit a narrow luminosity distribution in the J-band. The discrepancy with Li et al. [86] ($H_0 = 74.7 \pm 3.1$) appears to originate from differences in:

- JAGB zero-point calibration (LMC anchor treatment)
- Photometric selection criteria for carbon stars
- Assumed shape of the JAGB luminosity function

This measurement highlights that even within a single indicator class, methodological choices can lead to $\sim 7 \text{ km s}^{-1} \text{ Mpc}^{-1}$ differences in inferred H_0 .

d. *Wagner et al.*

The measurement by Wagner et al. [165] (2025) reports $H_0 = 63 \pm 6 \text{ km s}^{-1} \text{ Mpc}^{-1}$ using the local expansion parameter $\kappa = 1.4$, based on the infall velocity relation $v_{\text{inf}} = \kappa \cdot H_0 r$. However, the choice of $k = 1.4$ appears somewhat arbitrary; standard models of the local Hubble flow typically adopt $\kappa \approx 1.2$. Since $H_0 \propto 1/\kappa$, adopting $\kappa = 1.3 \pm 0.1$ —a value intermediate between the theoretical expectation and the assumed value—would yield $H_0 \approx 68_{-8}^{+8} \text{ km s}^{-1} \text{ Mpc}^{-1}$, shifting the result toward the Planck value and closer to the Distance Ladder mean value. The systematic uncertainty in κ propagates directly into H_0 but this source of error was not included in the original analysis [165]. However, we do include this effect in our analysis and the data shown in Table X.

e. *Zhang et al.:pairwise velocities*

Zhang et al. (2024) [76] measured the Hubble constant using galaxy pairwise peculiar velocities from the Cosmicflows-4 catalog, obtaining $H_0 = 75.5 \pm 1.4 \text{ km s}^{-1} \text{ Mpc}^{-1}$ (statistical). However, as discussed in [76], several systematic uncertainties are not fully accounted for in the reported error budget. The distance calibration of CF-4 galaxies introduces uncertainties of $\sim 2\text{--}3\%$, translating to $\sim 1.5\text{--}2.3 \text{ km s}^{-1} \text{ Mpc}^{-1}$ in H_0 . The halo mass matching between simulations and observations, which is crucial for their method, contributes an estimated systematic error of $\sim 1\text{--}2\%$ ($\sim 0.8\text{--}1.5 \text{ km s}^{-1} \text{ Mpc}^{-1}$). Additionally, the modeling of pairwise velocities in the non-linear regime, where theoretical predictions are less certain, introduces uncertainties of $\sim 2\text{--}3\%$ ($\sim 1.5\text{--}2.3 \text{ km}$

$\text{s}^{-1} \text{ Mpc}^{-1}$). The choice of the maximum separation scale ($r_{\text{max}} = 16 \text{ Mpc}$) and the selection of the velocity threshold v_{max} add further systematic uncertainties of order $\sim 1\%$ ($\sim 0.8 \text{ km s}^{-1} \text{ Mpc}^{-1}$). Cosmic variance, despite mitigation through multiple simulation realizations, remains a source of systematic error. Combining these contributions in quadrature yields a total systematic uncertainty of approximately $\sim 3\text{--}4 \text{ km s}^{-1} \text{ Mpc}^{-1}$, which is comparable to or larger than the quoted statistical uncertainty. Therefore, a more complete error budget would be $H_0 = 75.5 \pm 1.4_{\text{stat}} \pm 3.5_{\text{sys}} \text{ km s}^{-1} \text{ Mpc}^{-1}$, or equivalently $H_0 = 75.5 \pm 3.8 \text{ km s}^{-1} \text{ Mpc}^{-1}$ when statistical and systematic errors are combined in quadrature. This corrected level of uncertainty is used in our analysis.

2. Key DLI–SHF Measurements

a. *TDCOSMO: Evolution of Strong Lensing Constraints*

The Time-Delay Cosmography (TDCOSMO) collaboration has produced a series of Strong Lensing H_0 measurements that illustrate the critical importance of lens mass modeling.

HOLiCOW (Millon et al. 2020): The original analysis yielded $H_0 = 74.2 \pm 1.6 \text{ km s}^{-1} \text{ Mpc}^{-1}$, assuming power-law mass profiles. This result was in 5σ tension with Planck.

TDCOSMO IV (Birrer et al. 2020): [191] Incorporating stellar kinematics to constrain the mass-sheet degeneracy (MSD) shifted the result to $H_0 = 67.4_{-3.2}^{+4.1} \text{ km s}^{-1} \text{ Mpc}^{-1}$ —now consistent with Planck. This dramatic shift demonstrated that power-law profiles alone cannot break the MSD.

Recent results (2023–2025): Subsequent analyses using hierarchical modeling, additional lens systems, and improved kinematics yield H_0 in the range $65\text{--}72 \text{ km s}^{-1} \text{ Mpc}^{-1}$, depending on modeling assumptions [95, 97].

We exclude the original Millon et al. (2020) result from our compilation because its methodology is now recognized as insufficient for robust H_0 inference.

We exclude the original Pesce et al. measurement from our sample, as the more recent Barua et al. analysis uses the same underlying data while addressing the known systematic uncertainties of the earlier measurement.

b. *Liu et al. (2023): SDSS J1004+4112 Cluster Lens*

The Liu et al. [101] analysis of the cluster-lensed quasar SDSS J1004+4112 explores 16 different mass models, yielding H_0 values spanning $55\text{--}90 \text{ km s}^{-1} \text{ Mpc}^{-1}$. Their combined constraint with equal weighting gives $H_0 = 67.5_{-8.9}^{+14.5} \text{ km s}^{-1} \text{ Mpc}^{-1}$.

In our analysis, we adopt their more constrained result of $H_0 = 59.1_{-3.5}^{+3.6} \text{ km s}^{-1} \text{ Mpc}^{-1}$, which corresponds to their selection of the two mass models (m113 and m123)

that best reproduce the observed shapes of the lensed quasar host galaxy and background galaxies (see their Figure 5 and Section V). The authors themselves emphasize this as a more physically motivated constraint, stating that these models “best match the observed shapes.”

We acknowledge that this choice favors the lower H_0 value. However, selecting mass models based on their ability to reproduce independent observables (lensed galaxy morphologies) is more principled than equal weighting of all models regardless of their physical plausibility. Readers should note that the conservative combined result ($H_0 = 67.5^{+14.5}_{-8.9} \text{ km s}^{-1} \text{ Mpc}^{-1}$) remains consistent with our conclusions given its large uncertainty.

c. Kelly et al. (2023) and Li et al. (2024): SN Refsdal Time Delays

Supernova Refsdal, the first multiply-imaged supernova [192], provides unique advantages for time-delay cosmography: the supernova light curve allows unambiguous identification of multiple images, unlike quasar variability.

Both Kelly et al. [96] and Li et al. [113] analyze time delays from SN Refsdal, yet we classify them in different categories based on their methodological approaches:

Kelly et al. (2023) — Category 2: This analysis uses time delays from the “Einstein Cross” configuration plus the predicted reappearance of image “SX.” The result, $H_0 = 66.6^{+4.1}_{-3.3} \text{ km s}^{-1} \text{ Mpc}^{-1}$, is derived using specific cluster mass models that assume ΛCDM cosmology for the time-delay distance $D_{\Delta t}$ calculation and interprets results within the ΛCDM framework.

Li et al. (2024) — Category 3: This analysis explicitly develops a “cosmological-model-independent” approach, as emphasized in their title and methodology. They obtain $H_0 = 66.3^{+3.8}_{-3.6} \text{ km s}^{-1} \text{ Mpc}^{-1}$ using a combination of strong lensing and other probes to determine H_0 without assuming ΛCDM .

The distinction hinges on whether the original analysis explicitly states model-independence. While both measurements yield consistent H_0 values and analyze the same underlying data, their category assignments follow our classification criterion based on the authors’ stated assumptions. This example illustrates that identical data can yield measurements in different categories depending on the analysis methodology employed.

d. Piratova-Moreno et al.:FRBs

Piratova-Moreno et al. (2025) [99] employed Fast Radio Bursts (FRBs) as cosmological probes to measure the Hubble constant using a catalog of 98 localized FRBs. Using the Maximum Likelihood Estimate (MLE) method with confirmed FRBs, they obtained $H_0 = 65.13 \pm 2.52$

$\text{km s}^{-1} \text{ Mpc}^{-1}$ (statistical), while their mock FRB catalog yielded $H_0 = 67.30 \pm 0.91 \text{ km s}^{-1} \text{ Mpc}^{-1}$. However, this method is subject to substantial systematic uncertainties that are not fully quantified in the reported error budget. The primary systematic error arises from the decomposition of the observed dispersion measure (DM) into its constituent components: the Milky Way interstellar medium and halo (DM_{MW}), the intergalactic medium (DM_{IGM}), and the host galaxy (DM_{host}). The uncertainty in DM_{MW} depends on the Galactic electron density model used (NE2001 vs. YMW16), with differences of $\sim 20\%$ at low Galactic latitudes, contributing $\sim 1.5\text{--}2 \text{ km s}^{-1} \text{ Mpc}^{-1}$ to the H_0 uncertainty. The host galaxy contribution, DM_{host} , is highly uncertain and varies dramatically between FRBs—from $\sim 30 \text{ pc cm}^{-3}$ for typical hosts to over 900 pc cm^{-3} for extreme cases like FRB 20190520B. Studies suggest DM_{host} uncertainties of $\sim 50\text{--}100 \text{ pc cm}^{-3}$, which translate to systematic errors of $\sim 2\text{--}3 \text{ km s}^{-1} \text{ Mpc}^{-1}$ in H_0 . Additionally, the baryon fraction in the IGM (f_{IGM}) introduces further systematic uncertainty; recent estimates range from $f_{\text{IGM}} = 0.865^{+0.101}_{-0.165}$ to $0.93^{+0.04}_{-0.05}$, corresponding to $\sim 1\text{--}2 \text{ km s}^{-1} \text{ Mpc}^{-1}$ uncertainty in H_0 . The choice of $\text{DM}-z$ relation (linear vs. power-law) also significantly impacts results, with Piratova-Moreno et al. reporting values ranging from $H_0 = 51.27^{+3.80}_{-3.31} \text{ km s}^{-1} \text{ Mpc}^{-1}$ (linear) to $H_0 = 91.84 \pm 1.82 \text{ km s}^{-1} \text{ Mpc}^{-1}$ (power-law), indicating substantial model-dependent systematic uncertainties of order $\sim 5\text{--}15 \text{ km s}^{-1} \text{ Mpc}^{-1}$. Combining these systematic contributions in quadrature yields a total systematic error of approximately $\sim 6\text{--}8 \text{ km s}^{-1} \text{ Mpc}^{-1}$ for the MLE result, dominating over the statistical uncertainty. A more realistic error budget would therefore be $H_0 = 65.13 \pm 2.52_{\text{stat}} \pm 7_{\text{sys}} \text{ km s}^{-1} \text{ Mpc}^{-1}$, or equivalently $H_0 = 65.1 \pm 7.4 \text{ km s}^{-1} \text{ Mpc}^{-1}$ when combined in quadrature, reflecting the current limitations of FRB-based cosmology. This is the value used in our analysis.

e. Vogl et al. (2024): Tailored EPM

The Vogl et al. [112] tailored Expanding Photosphere Method represents the most precise cosmological-model-independent measurement supporting the high- H_0 solution outside the traditional distance ladder.

Method: EPM determines distances geometrically by combining photospheric angular size (from flux and temperature) with expansion velocity (from Doppler shifts). The “tailored” approach uses detailed NLTE radiative transfer models customized to individual SNe II in the redshift range $z \in [0.01, 0.04]$, rather than empirical dilution factors.

Result: $H_0 = 74.9 \pm 2.7 \text{ km s}^{-1} \text{ Mpc}^{-1}$, fully consistent with the Distance Ladder. In this measurement, the authors do not explicitly report the systematic uncertainties in their work. However, they estimate that the systematic errors are approximately of the same magnitude as the statistical ones, and we have adopted this

estimate in our analysis.

Significance: This measurement is independent of:

- SNe Ia physics (uses SNe II instead)
- Cepheid/TRGB calibrators (direct geometric distance)
- Λ CDM assumptions (no $H(z)$ integration required)

The agreement with the Distance Ladder suggests either a common systematic affecting both methods or that the high H_0 reflects true local physics.

Caveats: The method relies on supernova atmosphere modeling; current sample size is limited; further validation with independent codes is needed.

f. Barua et al. (2025): Megamaser Cosmology Project

The Megamaser Cosmology Project measures geometric distances to galaxies with circumnuclear water maser disks. The Barua et al. [73] frequentist analysis yields $H_0 = 73.5^{+3.0}_{-2.9} \text{ km s}^{-1} \text{ Mpc}^{-1}$.

Method: VLBI observations resolve the maser disk structure, providing angular diameter distances via Keplerian dynamics. The method is independent of stellar physics.

Classification note: We assign this measurement to Category 2 (Λ CDM-dependent) because it relies on the Λ CDM prediction for the angular diameter distance. Earlier MCP analyses that adopted SH0ES flow models for peculiar velocity corrections would be classified differently.

Evolution: Earlier measurements (Kuo 2013: 68 ± 9 ; Gao 2015: 66 ± 6) favored lower values with larger uncertainties.

g. Pogosian et al. (2024): Sound-Horizon-Free BAO

The Pogosian et al. [118] analysis demonstrates that H_0 can be constrained from BAO data without assuming the CMB Sound Horizon.

Method: Instead of using r_s as a standard ruler, this analysis treats r_s as a free parameter and constrains H_0 through:

- The shape of $H(z)$ from BAO peak positions
- Big Bang Nucleosynthesis constraints on ω_b
- The matter-radiation equality scale k_{eq}

Results: DESI BAO DR2 yields $H_0 = 69.37 \pm 0.65 \text{ km s}^{-1} \text{ Mpc}^{-1}$; pre-DESI BAO yields $H_0 = 68.05 \pm 0.94 \text{ km s}^{-1} \text{ Mpc}^{-1}$. The DESI DR2 result was presented by L. Pogosian during the CosmoVerse Seminar Series [121] and represents an update of [118] using DESI DR1 BAO data; publication is forthcoming.

Significance: These measurements anchor the low- H_0 solution in Category 4. Their high precision ($\sim 1.4\%$) means they dominate the weighted mean of this category.

h. Gravitational Wave standard sirens

GW standard sirens provide H_0 constraints independent of electromagnetic distance ladder:

Bright sirens (GW170817): The binary neutron star merger with optical counterpart yields $H_0 = 75.46^{+5.34}_{-5.39} \text{ km s}^{-1} \text{ Mpc}^{-1}$ [92], limited by the peculiar velocity of NGC 4993 and viewing angle degeneracy. Additionally, Wang et al. (2025) [193] find a consistent value of $H_0 = 72.57^{+4.09}_{-4.17} \text{ km s}^{-1} \text{ Mpc}^{-1}$. These measurements provide important complementary constraints that are independent of the Distance Ladder.

Dark sirens (GWTC-3): Statistical analysis of 47 events without counterparts yields $H_0 = 68^{+8}_{-6} \text{ km s}^{-1} \text{ Mpc}^{-1}$ [93], consistent with Planck.

The weighted mean of all GW measurements ($H_0 \approx 68 \pm 2 \text{ km s}^{-1} \text{ Mpc}^{-1}$) supports the low- H_0 solution, though with larger uncertainties than other probes.

i. Fast Radio Burst Measurements

FRB H_0 measurements use the dispersion measure-redshift relation to probe the cosmic baryon distribution:

Challenges: Significant systematic uncertainties arise from:

- Host galaxy DM contribution (poorly constrained)
- IGM density fluctuations
- Sample selection effects
- Galactic electron density models

Results: Published values span $H_0 \sim 65\text{--}86 \text{ km s}^{-1} \text{ Mpc}^{-1}$. Maximum-likelihood approaches [99] tend to favor lower values ($H_0 \approx 65 \text{ km s}^{-1} \text{ Mpc}^{-1}$). Also the estimation of H_0 using Fast Radio Bursts (FRBs) is highly sensitive to the model adopted for the Galactic electron density distribution. As highlighted by recent studies (e.g., Wang et al. [194]), switching between established models (such as NE2001 and YMW16) can shift the inferred H_0 value significantly (e.g., from ~ 69 to $\sim 75.6 \text{ km s}^{-1} \text{ Mpc}^{-1}$), introducing a systematic uncertainty that rivals the statistical error. As FRB samples grow and host DM distributions become better characterized, this probe may provide competitive constraints.

Appendix C: Correlation Matrix Estimates

A fundamental assumption of the weighted mean analysis in Section III is that measurements within each category are statistically independent. This assumption is violated to varying degrees due to shared calibration data,

common analysis frameworks, and overlapping samples. Here we assess the impact of correlations on our conclusions.

1. Sources of Correlation

a. Distance Ladder Correlations

Category 1 measurements share several inputs that induce positive correlations:

- **Geometric anchors:** Most Cepheid measurements use NGC 4258, LMC, and/or MW parallaxes. The anchor uncertainties propagate coherently.
- **SNe Ia samples:** Hubble-flow SNe Ia are predominantly from Pantheon+ [195], with substantial overlap. Standardization parameters (α , β , σ_{int}) are often shared.
- **Period–luminosity relations:** Cepheid analyses adopt similar functional forms and metallicity corrections.
- **Crowding corrections:** HST analyses use similar artificial star tests.

We estimate an effective correlation coefficient $\bar{\rho} \approx 0.3\text{--}0.5$ for typical pairs of Distance Ladder measurements.

b. DLI–SHF Correlations

Categories 2, 3, and 4 exhibit weaker correlations due to methodological diversity, but some correlations exist:

- **Strong lensing:** Multiple analyses of the same system (e.g., SN Refsdal) share time delay data and are highly correlated.
- **Gravitational waves:** Analyses using overlapping GW events share strain data and waveform models.
- **FRBs:** Later analyses often include events from earlier samples.
- **Cosmological priors:** Many analyses assume flat ΛCDM with $\Omega_m \approx 0.3$, inducing weak correlations.

We estimate $\bar{\rho} \approx 0.1\text{--}0.2$ for the sample.

2. Methodology for Correlation-Adjusted Estimates

For correlated measurements, the generalized weighted mean and its uncertainty are:

$$\hat{H}_0 = \frac{\mathbf{w}^T \mathbf{C}^{-1} \mathbf{H}_0}{\mathbf{w}^T \mathbf{C}^{-1} \mathbf{w}}, \quad \sigma_{\hat{H}_0}^2 = \frac{1}{\mathbf{w}^T \mathbf{C}^{-1} \mathbf{w}}, \quad (\text{C1})$$

where \mathbf{C} is the covariance matrix with elements $C_{ij} = \rho_{ij}\sigma_i\sigma_j$. For simplicity, we adopt a uniform correlation structure within each category:

$$\rho_{ij} = \begin{cases} 1 & \text{if } i = j \\ \bar{\rho} & \text{if } i \neq j \end{cases} \quad (\text{C2})$$

3. Impact on Combined Constraints

a. Distance Ladder (Category 1)

With $\bar{\rho} = 0.4$:

$$H_0^{\text{ladder,corr}} = 72.30 \pm 0.57 \text{ km s}^{-1} \text{ Mpc}^{-1}, \quad (\text{C3})$$

compared to $72.73 \pm 0.39 \text{ km s}^{-1} \text{ Mpc}^{-1}$ under independence. The central value shifts by only $0.4 \text{ km s}^{-1} \text{ Mpc}^{-1}$ (within statistical uncertainty), but the uncertainty increases by $\sim 46\%$.

b. Combined (Categories 2+3+4)

With $\bar{\rho} = 0.15$:

$$H_0^{\text{ladder-Indep.,corr}} = 69.52 \pm 0.42 \text{ km s}^{-1} \text{ Mpc}^{-1}, \quad (\text{C4})$$

compared to $69.37 \pm 0.34 \text{ km s}^{-1} \text{ Mpc}^{-1}$ under independence. The central value remains essentially unchanged, and the uncertainty increases by $\sim 22\%$.

c. Tension Between Categories

The correlation-adjusted tension is:

$$n_{\sigma}^{\text{corr}} = \frac{72.30 - 69.52}{\sqrt{0.57^2 + 0.42^2}} = 3.9\sigma. \quad (\text{C5})$$

This is reduced from 6.5σ under independence but remains highly significant.

4. Sensitivity Analysis

Table XII shows how the tension varies with assumed correlation strength.

TABLE XII. Sensitivity of tension significance to correlation assumptions.

$\bar{\rho}_{\text{ladder}}$	$\bar{\rho}_{\text{ladder-indep}}$	σ_{ladder}	$\sigma_{\text{ladder-indep}}$	Tension
0.0	0.00	0.39	0.34	6.5σ
0.2	0.10	0.60	0.42	3.9σ
0.4	0.15	0.57	0.42	3.9σ
0.5	0.20	0.53	0.41	4.1σ
0.6	0.25	0.48	0.40	4.3σ

Notes: Uncertainties in $\text{km s}^{-1} \text{Mpc}^{-1}$. Central values are relatively stable across correlation assumptions.

5. Conclusions from Correlation Analysis

Key findings:

1. **Central values are robust:** The weighted means shift by $\lesssim 1 \text{ km s}^{-1} \text{Mpc}^{-1}$ across plausible corre-

lation assumptions.

2. **Uncertainties increase:** Accounting for correlations increases uncertainties by 20–50%, depending on the assumed correlation strength.
3. **Tension remains significant:** For reasonable correlation estimates ($\bar{\rho}_{\text{ladder}} \sim 0.3\text{--}0.5$, $\bar{\rho}_{\text{one-step}} \sim 0.1\text{--}0.2$), the tension remains at the $4\text{--}5\sigma$ level.
4. **Qualitative conclusions unchanged:** The characterization of the Hubble tension as “Distance Ladder vs. The Rest” is robust to correlation modeling.

A fully rigorous treatment would require constructing the complete 88×88 covariance matrix from detailed assessment of shared data and methodology—a task beyond the scope of this work but warranted for future precision analyses.

[1] Planck Collaboration, N. Aghanim, *et al.*, Planck 2018 results. VI. Cosmological parameters, *Astron. Astrophys.* **641**, A6 (2020), arXiv:1807.06209 [astro-ph.CO].

[2] A. G. Riess, W. Yuan, L. M. Macri, D. Scolnic, D. Brout, S. Casertano, D. O. Jones, Y. Murakami, G. S. Anand, L. Breuval, T. G. Brink, A. V. Filippenko, S. Hoffmann, S. W. Jha, W. D. Kenworthy, J. Mackenty, B. E. Stahl, and W. Zheng, A Comprehensive Measurement of the Local Value of the Hubble Constant with $1 \text{ km s}^{-1} \text{Mpc}^{-1}$ Uncertainty from the Hubble Space Telescope and the SH0ES Team, *Astrophys. J. Lett.* **934**, L7 (2022), arXiv:2112.04510 [astro-ph.CO].

[3] A. G. Riess, S. Li, G. S. Anand, *et al.*, The Perfect Host: JWST Cepheid Observations in a Background-Free SN Ia Host Confirm No Bias in Hubble-Constant Measurements (2025), arXiv:2509.01667 [astro-ph.CO].

[4] S. Casertano *et al.*, The Local Distance Network, *Astrophys. J.* (2025), arXiv:2510.23823 [astro-ph.CO].

[5] E. Di Valentino, O. Mena, S. Pan, L. Visinelli, W. Yang, A. Melchiorri, D. F. Mota, A. G. Riess, and J. Silk, In the realm of the Hubble tension—a review of solutions, *Class. Quantum Grav.* **38**, 153001 (2021), arXiv:2103.01183 [astro-ph.CO].

[6] L. Knox and M. Millea, Hubble constant hunter’s guide, *Phys. Rev. D* **101**, 043533 (2020), arXiv:1908.03663 [astro-ph.CO].

[7] E. Abdalla *et al.*, Cosmology intertwined: A review of the particle physics, astrophysics, and cosmology associated with the cosmological tensions and anomalies, *JHEAp* **34**, 49 (2022), arXiv:2203.06142 [astro-ph.CO].

[8] L. Perivolaropoulos and F. Skara, Challenges for ΛCDM : An update, *New Astron. Rev.* **95**, 101659 (2022), arXiv:2105.05208 [astro-ph.CO].

[9] G. Alestas, L. Kazantzidis, and L. Perivolaropoulos, h_0 tension, phantom dark energy, and cosmological parameter degeneracies, *Physical Review D* **101**, 123516 (2020).

[10] M. S. Turner, Everyone wants something better than ΛCDM , arXiv preprint (2025), arXiv:2510.05483 [astro-ph.CO].

[11] H. Chaudhary, S. Capozziello, S. Praharaj, S. K. J. Pacif, and G. Mustafa, Is the ΛCDM model in crisis?, *JHEAp* **50**, 100507 (2026), arXiv:2509.17124 [gr-qc].

[12] L. Perivolaropoulos, The Challenges for ΛCDM and the Physics Transition Approaches, *Astrophys. Space Sci. Proc.* **1**, 181 (2025).

[13] M. Ruchika, W. Giarè, E. M. Teixeira, and A. Melchiorri, Resilience and implications of adiabatic CMB cooling, *Phys. Dark Univ.* **49**, 101999 (2025), arXiv:2505.02909 [astro-ph.CO].

[14] A. Smith, E. Özülker, E. Di Valentino, and C. van de Bruck, Dynamical Dark Energy Meets Varying Electron Mass: Implications for Phantom Crossing and the Hubble Constant, arXiv preprint arXiv:2510.21931 (2025), arXiv:2510.21931 [astro-ph.CO].

[15] V. Poulin, T. L. Smith, T. Karwal, and M. Kamionkowski, Early dark energy can resolve the hubble tension, *Physical Review Letters* **122**, 10.1103/physrevlett.122.221301 (2019).

[16] T. L. Smith, V. Poulin, J. L. Bernal, K. K. Boddy, M. Kamionkowski, and R. Murgia, Early dark energy is not excluded by current large-scale structure data, *Phys. Rev. D* **103**, 123542 (2021).

[17] T. L. Smith, V. Poulin, J. L. Bernal, K. K. Boddy, M. Kamionkowski, and R. Murgia, Early dark energy is not excluded by current large-scale structure data, *Physical Review D* **103**, 10.1103/physrevd.103.123542 (2021).

[18] K. Jedamzik, L. Pogosian, and G.-B. Zhao, Why reducing the cosmic sound horizon alone can not fully resolve the hubble tension, *Communications Physics* **4**, 10.1038/s42005-021-00628-x (2021).

[19] S. Vagnozzi, New physics in light of the H_0 tension: An alternative view, *Physical Review D* **102**, 10.1103/physrevd.102.023518 (2020).

[20] W. Giarè, O. Mena, E. Specogna, and E. Di Valentino, Neutrino mass tension or suppressed growth rate of matter perturbations?, *Phys. Rev. D* **112**, 103520 (2025), arXiv:2505.02909 [astro-ph.CO].

arXiv:2507.01848 [astro-ph.CO].

[21] F. Plaza, G. León, and L. Krasilburd, Probing the H_0 tension with holographic dark energy in unimodular gravity: insights from DESI DR2, *Eur. Phys. J. C* **85**, 1262 (2025), arXiv:2508.21175 [astro-ph.CO].

[22] H. Cheng, E. Di Valentino, L. A. Escamilla, A. A. Sen, and L. Visinelli, Pressure parametrization of dark energy: first and second-order constraints with latest cosmological data, *JCAP* **9** (9), 031, arXiv:2505.02932 [astro-ph.CO].

[23] S. Sánchez López, A. Karam, and D. K. Hazra, Non-Minimally Coupled Quintessence in Light of DESI, arXiv preprint arXiv:2510.14941 (2025), arXiv:2510.14941 [astro-ph.CO].

[24] C.-G. Park and B. Ratra, Updated observational constraints on ϕ CDM dynamical dark energy cosmological models, arXiv preprint arXiv:2509.25812 (2025), arXiv:2509.25812 [astro-ph.CO].

[25] A. J. Shajib and J. A. Frieman, Scalar-field dark energy models: Current and forecast constraints, *Phys. Rev. D* **112**, 063508 (2025), arXiv:2502.06929 [astro-ph.CO].

[26] L. A. Escamilla, E. Özülker, Ö. Akarsu, E. Di Valentino, and J. A. Vázquez, Do we need wavelets in the late Universe?, *Mon. Not. Roy. Astron. Soc.* **836**, 854 (2025), arXiv:2408.12516 [astro-ph.CO].

[27] E. Di Valentino, A. Melchiorri, O. Mena, and S. Vagnozzi, Interacting dark energy in the early 2020s: A promising solution to the H_0 and cosmic shear tensions, *Physics of the Dark Universe* **30**, 100666 (2020).

[28] E. Di Valentino, A. Melchiorri, O. Mena, and S. Vagnozzi, Nonminimal dark sector physics and cosmological tensions, *Physical Review D* **101**, 10.1103/physrevd.101.063502 (2020).

[29] D. H. Lee, W. Yang, E. Di Valentino, S. Pan, and C. van de Bruck, The Shape of Dark Energy: Constraining Its Evolution with a General Parametrization, arXiv (2025), arXiv:2507.11432 [astro-ph.CO].

[30] W. J. Wolf, C. García-García, and P. G. Ferreira, Robustness of dark energy phenomenology across different parameterizations, *JCAP* **5** (5), 34, arXiv:2502.04929 [astro-ph.CO].

[31] A. C. Ferri and A. Melchiorri, Can future CMB data discriminate between a cosmological constant and dynamical dark energy?, *JHEAp* **50**, 100504 (2025).

[32] E. Özülker, E. Di Valentino, and W. Giarè, Dark Energy Crosses the Line: Quantifying and Testing the Evidence for Phantom Crossing (2025), arXiv:2506.19053 [astro-ph.CO].

[33] E. Silva, M. A. Sabogal, M. Scherer, R. C. Nunes, E. Di Valentino, and S. Kumar, New constraints on interacting dark energy from DESI DR2 BAO observations, *Phys. Rev. D* **111**, 123511 (2025), arXiv:2503.23225 [astro-ph.CO].

[34] D. Efstratiou, E. Achilleas Paraskevas, and L. Perivolaropoulos, Addressing the DESI DR2 Phantom-Crossing Anomaly and Enhanced H_0 Tension with Reconstructed Scalar-Tensor Gravity, arXiv e-prints 10.48550/arXiv.2511.04610 (2025).

[35] S. Nojiri, S. D. Odintsov, and V. K. Oikonomou, Apparent Phantom Crossing in Gauss-Bonnet Gravity, arXiv e-prints (2025), arXiv:2512.06279 [gr-qc].

[36] M. Scherer, M. A. Sabogal, R. C. Nunes, and A. De Felice, Challenging the Λ CDM model: 5σ evidence for a dynamical dark energy late-time transition, *Phys. Rev. D* **112**, 043513 (2025), arXiv:2504.20664 [astro-ph.CO].

[37] M. Abdul Karim *et al.* (DESI), DESI DR2 results. II. Measurements of baryon acoustic oscillations and cosmological constraints, *Phys. Rev. D* **112**, 083515 (2025), arXiv:2503.14738 [astro-ph.CO].

[38] D. Pedrotti, L. A. Escamilla, V. Marra, L. Perivolaropoulos, and S. Vagnozzi, BAO miscalibration cannot rescue late-time solutions to the Hubble tension (2025), arXiv:2510.01974 [astro-ph.CO].

[39] D. Efstratiou and L. Perivolaropoulos, Metastable cosmological constant and gravitational bubbles: Ultralate-time transitions in modified gravity, *Phys. Rev. D* **111**, 123546 (2025), arXiv:2503.11365 [gr-qc].

[40] S. H. Mirpoorian, K. Jedamzik, and L. Pogosian, Is Dynamical Dark Energy Necessary? DESI BAO and Modified Recombination (2025), arXiv:2504.15274 [astro-ph.CO].

[41] S. Capozziello, H. Chaudhary, T. Harko, and G. Mustafa, Is Dark Energy Dynamical in the DESI Era? A Critical Review, arXiv (2025), arXiv:2512.10585 [astro-ph.CO].

[42] T.-N. Li, G.-H. Du, Y.-H. Li, Y. Li, J.-L. Ling, J.-F. Zhang, and X. Zhang, Updated constraints on interacting dark energy: A comprehensive analysis using multiple CMB probes, DESI DR2, and supernovae observations, arXiv (2025), arXiv:2510.11363 [astro-ph.CO].

[43] E. Ó. Colgáin, S. Pourojaghi, M. M. Sheikh-Jabbari, and L. Yin, How much has DESI dark energy evolved since DR1?, arXiv (2025), arXiv:2504.04417 [astro-ph.CO].

[44] S. Roy Choudhury, Cosmology in Extended Parameter Space with DESI Data Release 2 Baryon Acoustic Oscillations: A 2σ + Detection of Nonzero Neutrino Masses with an Update on Dynamical Dark Energy and Lensing Anomaly, *Astrophys. J. Lett.* **986**, L31 (2025), arXiv:2504.15340 [astro-ph.CO].

[45] M. Berti, E. Bellini, C. Bonvin, M. Kunz, M. Viel, and M. Zumalacarregui, Reconstructing the dark energy density in light of DESI BAO observations, *Phys. Rev. D* **112**, 023518 (2025), arXiv:2503.13198 [astro-ph.CO].

[46] X. D. Jia, J. P. Hu, D. H. Gao, S. X. Yi, and F. Y. Wang, The Hubble Tension Resolved by the DESI Baryon Acoustic Oscillations Measurements, *Astrophys. J. Lett.* **994**, L22 (2025), arXiv:2509.17454 [astro-ph.CO].

[47] Y.-M. Zhang, T.-N. Li, G.-H. Du, S.-H. Zhou, L.-Y. Gao, J.-F. Zhang, and X. Zhang, Alleviating the h_0 tension through new interacting dark energy model in light of desi dr2 (2025), arXiv:2510.12627 [astro-ph.CO].

[48] G. Alestas, L. Kazantzidis, and L. Perivolaropoulos, $w-m$ phantom transition at $z_t < 0.1$ as a resolution of the hubble tension, *Physical Review D* **103**, 083517 (2021).

[49] E. Silva and R. C. Nunes, Testing signatures of phantom crossing through full-shape galaxy clustering analysis, *JCAP* **11** (11), 078, arXiv:2507.13989 [astro-ph.CO].

[50] I. D. Gialamas, G. Hütsi, M. Raidal, J. Urrutia, M. Vasar, and H. Veermäe, Quintessence and phantoms in light of DESI 2025, *Phys. Rev. D* **112**, 63551 (2025), arXiv:2506.21542 [astro-ph.CO].

[51] N. Roy and S. Chakrabarti, Is Phantom Barrier Crossing Inevitable? A Cosmographic Analysis, arXiv e-prints (2025), arXiv:2508.13740 [astro-ph.CO].

[52] F. B. M. d. Santos, J. Moraes, S. Pan, W. Yang,

and E. Di Valentino, A New Window on Dynamical Dark Energy: Combining DESI-DR2 BAO with future Gravitational Wave Observations, arXiv (2025), [arXiv:2504.04646 \[astro-ph.CO\]](#).

[53] M. A. Abchouyeh and M. H. P. M. van Putten, Evidence for increasing dark energy in DESI from the Local Distance Ladder, in *21st Rencontres du Vietnam: Flavour Physics Conference 2025* (2025) [arXiv:2509.23168 \[astro-ph.CO\]](#).

[54] V. Marra and L. Perivolaropoulos, Rapid transition of g_{eff} at $z_t \simeq 0.01$ as a possible solution of the hubble and growth tensions, *Physical Review D* **104**, L021303 (2021).

[55] Ruchika, L. Perivolaropoulos, and A. Melchiorri, Effects of a local physics change on the h_0 es determination of h_0 , arXiv preprint (2025), [arXiv:2408.03875 \[astro-ph.CO\]](#).

[56] L. Perivolaropoulos and Ruchika, Hubble Tension and the G-step Model: Re-examination of Recent Constraints on Modified Local Physics (2025), [arXiv:2508.04395 \[astro-ph.CO\]](#).

[57] L. Perivolaropoulos, Is the Hubble Crisis Connected with the Extinction of Dinosaurs?, *Universe* **8**, 263 (2022), [arXiv:2201.08997 \[astro-ph.EP\]](#).

[58] H. Desmond, B. Jain, and J. Sakstein, Local resolution of the Hubble tension: The impact of screened fifth forces on the cosmic distance ladder, *Phys. Rev. D* **100**, 043537 (2019), [Erratum: *Phys. Rev. D* 101, 069904 (2020), Erratum: *Phys. Rev. D* 101, 129901 (2020)], [arXiv:1907.03778 \[astro-ph.CO\]](#).

[59] H. Desmond and J. Sakstein, Screened fifth forces lower the TRGB-calibrated Hubble constant too, *Phys. Rev. D* **102**, 023007 (2020), [arXiv:2003.12876 \[astro-ph.CO\]](#).

[60] M. Höglås, E. Mörtsell, H. Desmond, and A. Riess, Constraining Fifth Forces using the Local Distance Ladder: Implications for the Hubble Tension, arXiv preprint (2025), [arXiv:2512.14814 \[astro-ph.CO\]](#).

[61] W. D. Kenworthy, D. Scolnic, and A. Riess, The Local Perspective on the Hubble Tension: Local Structure Does Not Impact Measurement of the Hubble Constant, *The Astrophysical Journal* **875**, 145 (2019), [arXiv:1901.08681 \[astro-ph.CO\]](#).

[62] V. V. Luković, B. S. Haridasu, and N. Vittorio, Exploring the evidence for a large local void with supernovae Ia data, *Monthly Notices of the Royal Astronomical Society* **491**, 2075 (2020), [arXiv:1907.11219 \[astro-ph.CO\]](#).

[63] R.-G. Cai, J.-F. Ding, Z.-K. Guo, S.-J. Wang, and W.-W. Yu, Do the observational data favor a local void?, *Physical Review D* **103**, 123539 (2021), [arXiv:2012.12692 \[astro-ph.CO\]](#).

[64] S. Castello, M. Höglås, and E. Mörtsell, A cosmological underdensity does not solve the Hubble tension, *Journal of Cosmology and Astroparticle Physics* **2022** (07), 003, [arXiv:2110.04226 \[astro-ph.CO\]](#).

[65] D. Camarena, V. Marra, Z. Sakr, and C. Clarkson, A void in the Hubble tension? The end of the line for the Hubble bubble, *Classical and Quantum Gravity* **39**, 184001 (2022), [arXiv:2205.05422 \[astro-ph.CO\]](#).

[66] V. Marra, T. Castro, D. Camarena, S. Borgani, and A. Ragagnin, Not Empty Enough: A Local Void Cannot not Solve the H_0 Tension, in *Modified and Quantum Gravity*, Lecture Notes in Physics, Vol. 1017, edited by R. Ferraro and S. Ferraro (Springer, 2023) pp. 409–423, [arXiv:2309.05749 \[astro-ph.CO\]](#).

[67] J.-Y. Jia, H. Wei, *et al.*, Alleviating the Hubble Tension with a Local Void and Transitions of the Absolute Magnitude, *Physical Review D* **112**, 043507 (2025), [arXiv:2504.13380 \[astro-ph.CO\]](#).

[68] I. Banik and V. Kalaitzidis, Testing the local void hypothesis using baryon acoustic oscillation measurements over the last twenty years, *Mon. Not. Roy. Astron. Soc.* **10.1093/mnras/staf781** (2025), [arXiv:2501.17934 \[astro-ph.CO\]](#).

[69] L. Perivolaropoulos, Hubble tension or distance ladder crisis?, *Phys. Rev. D* **110**, 123518 (2024).

[70] L. Huang, R.-G. Cai, S.-J. Wang, J.-Q. Liu, and Y.-H. Yao, Narrowing down the Hubble tension to the first two rungs of distance ladders, *Sci. China Phys. Mech. Astron.* **68**, 280405 (2025), [arXiv:2410.06053 \[astro-ph.CO\]](#).

[71] D. Pedrotti, J.-Q. Jiang, L. A. Escamilla, S. S. da Costa, and S. Vagnozzi, Multidimensionality of the Hubble tension: The roles of Ωm and ωc , *Phys. Rev. D* **111**, 023506 (2025), [arXiv:2408.04530 \[astro-ph.CO\]](#).

[72] C. Y. Kuo, J. A. Braatz, M. J. Reid, *et al.*, The Megamaser Cosmology Project. V. An Angular-diameter Distance to NGC 6264 at 140 Mpc, *Astrophys. J.* **767**, 155 (2013).

[73] S. Barua *et al.*, Megamaser Cosmology Project: An updated constraint on H_0 (2025), [arXiv:2502.11998 \[astro-ph.CO\]](#).

[74] E. Di Valentino *et al.* (CosmoVerse Network), The CosmoVerse White Paper: Addressing observational tensions in cosmology with systematics and fundamental physics, *Phys. Dark Univ.* **49**, 101965 (2025), [arXiv:2504.01669 \[astro-ph.CO\]](#).

[75] W. L. Freedman *et al.*, Status Report on the Chicago-Carnegie Hubble Program (CCHP): Three Independent Astrophysical Determinations of the Hubble Constant Using the James Webb Space Telescope (2024), [arXiv:2408.06153 \[astro-ph.CO\]](#).

[76] W. Zhang, M.-c. Chu, S. Liao, S. Yeung, and H.-J. Hu, Measuring the Hubble Constant through the Galaxy Pairwise Peculiar Velocity, *Astrophys. J. Lett.* **978**, L6 (2024).

[77] C. G. Tsagas, L. Perivolaropoulos, and K. Asvesta, Large-scale peculiar velocities in the universe, arXiv (2025), [arXiv:2510.05340 \[astro-ph.CO\]](#).

[78] C. Duangchan, A. Valade, N. I. Libeskind, and M. Steinmetz, Prior-free cosmological parameter estimation of Cosmicflows-4, arXiv (2025), [arXiv:2507.22236 \[astro-ph.CO\]](#).

[79] V. Salzano, J. Beltrán Jiménez, D. Bettoni, P. Brax, and A. Valade, Updates on dipolar anisotropy in local measurements of the Hubble constant from Cosmicflows-4, arXiv (2025), [arXiv:2512.02526 \[astro-ph.CO\]](#).

[80] C. D. Huang, A. G. Riess, W. Yuan, L. M. Macri, N. L. Zakamska, S. Casertano, P. A. Whitelock, S. L. Hoffmann, A. V. Filippenko, and D. Scolnic, Hubble Space Telescope Observations of Mira Variables in the SN Ia Host NGC 1559: An Alternative Candle to Measure the Hubble Constant, *Astrophys. J.* **889**, 5 (2020).

[81] T. de Jaeger, B. E. Stahl, W. Zheng, A. V. Filippenko, A. G. Riess, and L. Galbany, A measurement of the Hubble constant from Type II supernovae, *Mon. Not. R. Astron. Soc.* **496**, 3402 (2020), [arXiv:2006.03412 \[astro-ph.CO\]](#).

[82] N. Khetan, L. Izzo, M. Branchesi, *et al.*, A new measure-

ment of the Hubble constant using Type Ia supernovae calibrated with surface brightness fluctuations, *Astron. Astrophys.* **647**, A72 (2021), arXiv:2008.07754 [astro-ph.CO].

[83] W. L. Freedman, Measurements of the Hubble Constant: Tensions in Perspective, *Astrophys. J.* **919**, 16 (2021).

[84] W. D. Kenworthy *et al.*, Measurements of the hubble constant with a two rung distance ladder: Two out of three ain't bad, *Astrophys. J.* **935**, 83 (2022), arXiv:2204.10866 [astro-ph.CO].

[85] D. Scolnic, A. G. Riess, J. Wu, *et al.*, CATS: The Hubble Constant from Standardized TRGB and Type Ia Supernova Measurements, *Astrophys. J. Lett.* **954**, L31 (2024), arXiv:2304.06693 [astro-ph.CO].

[86] S. Li, A. G. Riess, S. Casertano, G. S. Anand, D. M. Scolnic, W. Yuan, L. Breuval, and C. D. Huang, Reconnaissance with JWST of the J-region Asymptotic Giant Branch in Distance Ladder Galaxies: From Irregular Luminosity Functions to Approximation of the Hubble Constant, *Astrophys. J.* **966**, 20 (2024).

[87] A. J. Lee, W. L. Freedman, B. F. Madore, I. S. Jang, K. A. Owens, and T. J. Hoyt, The Chicago-Carnegie Hubble Program: The JWST J-region Asymptotic Giant Branch (JAGB) Extragalactic Distance Scale, *Astrophys. J.* **956**, 15 (2024), arXiv:2408.03474 [astro-ph.GA].

[88] P. Ruiz-Lapuente, A. Quintana-Estellés, J. I. G. Hernández, and A. Pastorello, "sne ia twins" in the hubble flow, and the determination of h_0 (2025), arXiv:2512.02391 [astro-ph.CO].

[89] J. B. Jensen, J. P. Blakeslee, M. Cantiello, *et al.*, The TRGB-SBF Project. III. Refining the HST Surface Brightness Fluctuation Distance Scale Calibration with JWST, *Astrophys. J.* **987**, 87 (2025).

[90] A. Bhardwaj, N. Matsunaga, C. D. Huang, A. G. Riess, and M. Rejkuba, Absolute Calibration of Cluster Mira Variables to Provide a New Anchor for the Hubble Constant Determination (2025), arXiv:2507.10658 [astro-ph.GA].

[91] M. J. B. Newman, C. Larison, S. W. Jha, *et al.*, Tip of the Red Giant Branch Distances to NGC 1316, NGC 1380, NGC 1404, and NGC 4457 (2025), arXiv:2508.20023 [astro-ph.CO].

[92] A. Palmese, R. Kaur, A. Hajela, R. Margutti, A. McDowell, and A. MacFadyen, A standard siren measurement of the hubble constant using gw170817 and the latest observations of the electromagnetic counterpart afterglow (2023), arXiv:2305.19914 [astro-ph.CO].

[93] LIGO Scientific Collaboration and Virgo Collaboration, A Gravitational-wave Measurement of the Hubble Constant Following the Second Observing Run of Advanced LIGO and Virgo, *Astrophys. J.* **909**, 218 (2021), arXiv:1908.06060 [astro-ph.CO].

[94] F. Beirnaert *et al.*, Dark siren constraints on the Hubble constant from LIGO/Virgo O4 (2025), arXiv:2505.14077 [astro-ph.CO].

[95] A. J. Shajib, P. Mozumdar, G. C.-F. Chen, *et al.*, TD-COSMO: XII. Improved Hubble constant measurement from lensing time delays using spatially resolved stellar kinematics of the lens galaxy, *Astron. Astrophys.* **673**, A9 (2023).

[96] P. L. Kelly *et al.*, Constraints on the Hubble constant from Supernova Refsdal's reappearance, *Science* **380**, 1322 (2023), arXiv:2305.06367 [astro-ph.CO].

[97] TDCOSMO Collaboration, S. Birrer, *et al.*, TDCOSMO 2025: Cosmological constraints from strong lensing time delays (2025), arXiv:2506.03023 [astro-ph.CO].

[98] Q. Wu, G.-Q. Zhang, and F.-Y. Wang, An 8 per cent determination of the Hubble constant from localized fast radio bursts, *Mon. Not. R. Astron. Soc. Lett.* **515**, L1 (2022), arXiv:2108.00581 [astro-ph.CO].

[99] L. Piratova-Moreno *et al.*, Constraining the Hubble constant with fast radio bursts using a maximum likelihood estimator (2025), arXiv:2502.08509 [astro-ph.CO].

[100] K. Napier, K. Sharon, H. Dahle, *et al.*, Hubble Constant Measurement from Three Large-Separation Quasars Strongly Lensed by Galaxy Clusters, *Astrophys. J.* **944**, 71 (2023), arXiv:2301.11240 [astro-ph.CO].

[101] Y. Liu, M. Oguri, and S. Cao, Hubble constant from the cluster-lensed quasar system sdss j1004+4112: investigation of the lens model dependence (2023), arXiv:2307.14833 [astro-ph.CO].

[102] J. Martínez-Arrizabalaga, J. M. Diego, and L. J. Goicoechea, Parameter-free Hubble constant from the quadruply lensed quasar SDSS J1004+4112, *Astron. Astrophys.* **682**, A187 (2024).

[103] M. Pascale *et al.*, SN H0pe: The First Measurement of the Hubble Constant from a Multiply Imaged Type Ia Supernova, Discovered by JWST, *Astrophys. J.* **962**, 45 (2024), arXiv:2403.18902 [astro-ph.CO].

[104] Y.-P. Yang *et al.*, Constraining H_0 with FRB scattering (2024), arXiv:2411.02249 [astro-ph.CO].

[105] J. D. R. Pierel, E. E. Hayes, M. Millon, *et al.*, Cosmology with supernova Encore in the strong lensing cluster MACS J0138-2155: Time delays and Hubble constant measurement (2025), arXiv:2509.12301 [astro-ph.CO].

[106] S. H. Suyu *et al.*, Cosmology with supernova Encore in the strong lensing cluster MACS J0138-2155: Lens model comparison and H_0 measurement, arXiv (2025), arXiv:2509.12319 [astro-ph.CO].

[107] F. Gao, J. A. Braatz, M. J. Reid, *et al.*, The Megamaser Cosmology Project. VIII. A Geometric Distance to NGC 5765b, *Astrophys. J.* **817**, 128 (2016), arXiv:1511.08311 [astro-ph.CO].

[108] M. Moresco, Addressing the hubble tension with cosmic chronometers (2023), arXiv:2307.09501 [astro-ph.CO].

[109] J.-C. Zhang, K. Jiao, T. Zhang, T.-J. Zhang, and B. Yu, A Reliable Calibration of H II Galaxies Hubble Diagram with Cosmic Chronometers and Artificial Neural Network, *Astrophys. J.* **936**, 21 (2022).

[110] S.-S. Du, J.-J. Wei, Z.-Q. You, Z.-C. Chen, Z.-H. Zhu, and E.-W. Liang, Model-independent determination of H_0 and $\Omega_{K,0}$ using time-delay galaxy lenses and gamma-ray bursts, *Mon. Not. R. Astron. Soc.* **521**, 4963 (2023).

[111] A. Sneppen, D. Watson, D. Poznanski, O. Just, A. Bauswein, and R. Wojtak, Measuring the Hubble constant with kilonovae using the expanding photosphere method, *Astron. Astrophys.* **678**, A14 (2023).

[112] C. Vogl *et al.*, A Tailored Expanding Photosphere Method to Measure H_0 from Type II Supernovae (2024), arXiv:2411.04968 [astro-ph.CO].

[113] X. Li and K. Liao, Determining Cosmological-model-independent H_0 with Gravitationally Lensed Supernova Refsdal, *Astrophys. J.* **966**, 121 (2024).

[114] J.-Y. Song, J.-Z. Qi, J.-F. Zhang, and X. Zhang, Model-independent H_0 within FLRW: Joint Constraints from GWTC-3 Standard Sirens and Strong Lensing Time De-

lays, *Astrophys. J. Lett.* **985**, L44 (2025).

[115] A. Favale, A. Gómez-Valent, and M. Migliaccio, Revisiting model-independent constraints on spatial curvature and cosmic ladders calibration: updated and forecast analyses (2025), [arXiv:2511.19332 \[astro-ph.CO\]](#).

[116] O. H. E. Philcox, G. S. Farren, B. D. Sherwin, E. J. Baxter, and D. J. Brout, Determining the Hubble constant without the sound horizon: A 3.6% constraint on H_0 from galaxy surveys, CMB lensing, and supernovae, *Phys. Rev. D* **106**, 063530 (2022).

[117] B. Bahr-Kalus, D. Parkinson, *et al.*, Model-independent measurement of the matter-radiation equality scale in DESI 2024, *Phys. Rev. D* **112**, 6 (2025).

[118] L. Pogosian *et al.*, Measuring H_0 from DESI BAO without the Sound Horizon (2024), [arXiv:2405.20306 \[astro-ph.CO\]](#).

[119] E. D. Reese, Measuring the Hubble Constant with the Sunyaev-Zel'dovich Effect, arXiv e-prints (2003), [arXiv:astro-ph/0306073](#).

[120] L. Colaço *et al.*, A hubble constant estimate from galaxy cluster and type ia sne observations (2023), [arXiv:2310.18711 \[astro-ph.CO\]](#).

[121] L. Pogosian, Sound-horizon-agnostic approaches to the Hubble tension, CosmoVerse Seminar Series, CosmoVerse COST Action (2025), presented in September 2025. Online seminar discussing updated BMB acoustic consistency tests and DESI BAO results. Reference to $H_0 = 69.37 \pm 0.65$ km/s/Mpc result.

[122] H. García Escudero, S. H. Mirpoorian, and L. Pogosian, Sound-horizon-agnostic inference of the hubble constant and neutrino mass from bao, cmb lensing, and galaxy weak lensing and clustering, arXiv e-prints (2025), [arXiv:2509.16202 \[astro-ph.CO\]](#).

[123] E. A. Zaborowski *et al.*, H_0 Without the Sound Horizon (or Supernovae): A 2% Measurement in DESI DR1, arXiv (2025), [arXiv:2510.19149 \[astro-ph.CO\]](#).

[124] A. Krolewski, A. Crespi, W. J. Percival, *et al.*, A measurement of H_0 from DESI DR1 using energy densities (2025), [arXiv:2511.23432 \[astro-ph.CO\]](#).

[125] J. P. Blakeslee, J. B. Jensen, C.-P. Ma, P. A. Milne, and J. E. Greene, The Hubble Constant from Infrared Surface Brightness Fluctuation Distances, *Astrophys. J.* **911**, 65 (2021).

[126] I. Banik and N. Samaras, Constraints on the Hubble and matter density parameters with and without modelling the CMB anisotropies, *Astronomy* **4**, 24 (2025), [arXiv:2410.00804 \[astro-ph.CO\]](#).

[127] M. Högas and E. Mörtsell, Bimetric gravity improves the fit to DESI BAO and eases the Hubble tension, *Phys. Rev. D* **112**, 103515 (2025), [arXiv:2507.03743 \[astro-ph.CO\]](#).

[128] F. Plaza and L. Kraiselburd, Testing $f(R)$ -gravity models with DESI DR2 2025-BAO and other cosmological data, *Phys. Rev. D* **112**, 023554 (2025), [arXiv:2504.05432 \[gr-qc\]](#).

[129] S. D. Odintsov, V. K. Oikonomou, and G. S. Sharov, Dynamical dark energy from F(R) gravity models unifying inflation with dark energy: Confronting the latest observational data, *JHEAp* **50**, 100471 (2026), [arXiv:2506.02245 \[gr-qc\]](#).

[130] J. Pan and G. Ye, Non-minimally coupled gravity constraints from DESI DR2 data, arXiv (2025), [arXiv:2503.19898 \[astro-ph.CO\]](#).

[131] Ö. Akarsu, L. Perivolaropoulos, A. Tsikounoudoura, A. E. Yi̇kselci, and A. Zhuk, Dynamical dark energy with AdS-to-dS and dS-to-dS transitions: Implications for the H_0 tension, arXiv e-prints (2025), [arXiv:2502.14667 \[astro-ph.CO\]](#).

[132] G. Alestas, D. Camarena, E. Di Valentino, L. Kazantzidis, V. Marra, S. Nesseris, and L. Perivolaropoulos, Late-transition versus smooth $H(z)$ -deformation models for the resolution of the Hubble crisis, *Phys. Rev. D* **105**, 063538 (2022), [arXiv:2110.04336 \[astro-ph.CO\]](#).

[133] L. Perivolaropoulos and F. Skara, A Reanalysis of the Latest SH0ES Data for H_0 : Effects of New Degrees of Freedom on the Hubble Tension, *Universe* **8**, 502 (2022), [arXiv:2208.11169 \[astro-ph.CO\]](#).

[134] D. W. Pesce *et al.*, The Megamaser Cosmology Project. XIII. Combined Hubble constant constraints, *Astrophys. J. Lett.* **891**, L1 (2020).

[135] B. W. Silverman, *Density Estimation for Statistics and Data Analysis*, Monographs on Statistics and Applied Probability (Chapman & Hall, London, 1986).

[136] L. Perivolaropoulos and F. Skara, Hubble tension or a transition of the Cepheid SnIa calibrator parameters?, *Phys. Rev. D* **104**, 123511 (2021), [arXiv:2109.04406 \[astro-ph.CO\]](#).

[137] M. K. Sharma, L. Perivolaropoulos, and M. Sami, Multi-Parameter Transitions in Cosmological Calibrators: A Resolution to the Hubble Tension from SH0ES Data Analysis, arXiv preprint (2025), [arXiv:2504.19807 \[astro-ph.CO\]](#).

[138] H. Desmond, R. Stiskalek, J. A. Najera, and I. Banik, The subtle statistics of the distance ladder: On the distance prior and selection effects, arXiv preprint (2025), [arXiv:2511.03394 \[astro-ph.CO\]](#).

[139] O. Akarsu, A. D. Felice, E. D. Valentino, S. Kumar, R. C. Nunes, E. Ozulker, J. A. Vazquez, and A. Yadav, Λ_s CDM cosmology from a type-II minimally modified gravity (2025), [arXiv:2402.07716 \[astro-ph.CO\]](#).

[140] Ö. Akarsu, A. Çam, E. A. Paraskevas, and L. Perivolaropoulos, Linear matter density perturbations in the Λ_s CDM model: Examining growth dynamics and addressing the S_8 tension, *Journal of Cosmology and Astroparticle Physics* **2025** (08), 089.

[141] E. Specogna, S. A. Adil, E. Ozulker, E. Di Valentino, R. C. Nunes, O. Akarsu, and A. A. Sen, Updated Constraints on Omnipotent Dark Energy: A Comprehensive Analysis with CMB and BAO Data, arXiv (2025), [arXiv:2504.17859 \[gr-qc\]](#).

[142] DESI Collaboration, DESI 2024 VI: Cosmological Constraints from the Measurements of Baryon Acoustic Oscillations (2024), [arXiv:2404.03002 \[astro-ph.CO\]](#).

[143] W. Giare, T. Mahassen, E. Di Valentino, and S. Pan, An overview of what current data can (and cannot yet) say about evolving dark energy, *Phys. Dark Univ.* **48**, 101906 (2025), [arXiv:2502.10264 \[astro-ph.CO\]](#).

[144] Q. Gao, Z. Peng, S. Gao, and Y. Gong, On the Evidence of Dynamical Dark Energy, *Universe* **11**, 10 (2025), [arXiv:2411.16046 \[astro-ph.CO\]](#).

[145] Colgáin, Eoin Ó and Sheikh-Jabbari, M. M. and Solomon, R. and Bargiacchi, G. and Capozziello, S. and Dainotti, M. G. and Stojkovic, D., "Revealing intrinsic flat Λ CDM biases with standardizable candles", *Phys. Rev. D* **106**, L041301 (2022), [arXiv:2203.10558 \[astro-ph.CO\]](#).

ph.CO].

[146] E. Ó. Colgáin and M. M. Sheikh-Jabbari, DESI and SNe: Dynamical Dark Energy, Ω_m Tension or Systematics?, *Mon. Not. Roy. Astron. Soc.* **542**, L24 (2025), [arXiv:2412.12905 \[astro-ph.CO\]](#).

[147] A. Theodoropoulos and L. Perivolaropoulos, The hubble tension, the m crisis of late time $h(z)$ deformation models and the reconstruction of quintessence lagrangians, *Universe* **7**, 300 (2021).

[148] L. Perivolaropoulos and F. Skara, On the homogeneity of SNIa absolute magnitude in the Pantheon+ sample, *Mon. Not. Roy. Astron. Soc.* **520**, 5110 (2023), [arXiv:2301.01024 \[astro-ph.CO\]](#).

[149] M. Lopez-Hernandez, E. Ó. Colgáin, S. Pourojaghi, and M. M. Sheikh-Jabbari, Crosschecking Cosmic Distances from DESI BAO and DES SNe Points to Systematics, *arXiv* (2025), [arXiv:2510.04179 \[astro-ph.CO\]](#).

[150] E. M. Teixeira, W. Giarè, N. B. Hogg, T. Montandon, A. Poudou, and V. Poulin, Implications of distance duality violation for the H_0 tension and evolving dark energy, *Phys. Rev. D* **112**, 023515 (2025), [arXiv:2504.10464 \[astro-ph.CO\]](#).

[151] A. G. Abac *et al.* (LIGO Scientific, VIRGO, KAGRA), GWTC-4.0: Constraints on the Cosmic Expansion Rate and Modified Gravitational-wave Propagation (2025), [arXiv:2509.04348 \[astro-ph.CO\]](#).

[152] T. Louis *et al.* (Atacama Cosmology Telescope), The Atacama Cosmology Telescope: DR6 power spectra, likelihoods and Λ CDM parameters, *JCAP* **11** (11), 062, [arXiv:2503.14452 \[astro-ph.CO\]](#).

[153] E. Calabrese *et al.* (Atacama Cosmology Telescope), The Atacama Cosmology Telescope: DR6 constraints on extended cosmological models, *JCAP* **11** (11), 063, [arXiv:2503.14454 \[astro-ph.CO\]](#).

[154] E. Kourkchi, R. B. Tully, G. S. Anand, H. M. Courtois, A. Dupuy, J. D. Neill, L. Rizzi, and M. Seibert, Cosmicflows-4: The Calibration of Optical and Infrared Tully-Fisher Relations, *Astrophys. J.* **896**, 3 (2020).

[155] S. Dhawan, A. Goobar, J. Johansson, *et al.*, A Uniform Type Ia Supernova Distance Ladder with the Zwicky Transient Facility: Absolute Calibration Based on the Tip of the Red Giant Branch Method, *Astrophys. J.* **934**, 185 (2022).

[156] S. Dhawan, S. Thorp, K. S. Mandel, *et al.*, A BayeSN distance ladder: H_0 from a consistent modelling of Type Ia supernovae from the optical to the near-infrared, *Mon. Not. R. Astron. Soc.* **524**, 235 (2023).

[157] T. de Jaeger and L. Galbany, The Pursuit of the Hubble Constant Using Type II Supernovae (2023), [arXiv:2305.17243 \[astro-ph.CO\]](#).

[158] S. A. Uddin, C. R. Burns, M. M. Phillips, *et al.*, Carnegie Supernova Project-I and -II: Measurements of H_0 using Cepheid, TRGB, and SBF Distance Calibration to Type Ia Supernovae (2023), [arXiv:2308.01875 \[astro-ph.CO\]](#).

[159] C. D. Huang, W. Yuan, A. G. Riess, *et al.*, The Mira Distance to M101 and a 4 percent Measurement of H_0 , *Astrophys. J.* **963**, 83 (2024).

[160] R. Chávez, R. Terlevich, E. Terlevich, *et al.*, Mapping the Hubble Flow from $z \sim 0$ to $z \sim 7.5$ with HII Galaxies (2025), [arXiv:2404.16261 \[astro-ph.CO\]](#).

[161] P. Boubel, M. Colless, K. Said, and L. Staveley-Smith, An improved Tully-Fisher estimate of H_0 , *Mon. Not. R. Astron. Soc.* **533**, 1550 (2024).

[162] K. Said, C. Howlett, T. Davis, *et al.*, DESI peculiar velocity survey - Fundamental Plane, *Mon. Not. R. Astron. Soc.* **539**, 3627 (2025).

[163] R. Wojtak and J. Hjorth, Stretch to stretch, dust to dust: lower-value local H_0 measurement from two-population modelling of type Ia supernovae (2025), [arXiv:2506.22150 \[astro-ph.CO\]](#).

[164] R.-P. Kudritzki, F. Bresolin, M. A. Urbanek, and E. Sextl, Blue supergiants and the zero point of the Tully-Fisher relation (2025), [arXiv:2510.20652 \[astro-ph.CO\]](#).

[165] J. Wagner, D. Benisty, and I. D. Karachentsev, The Binary Ballet: Mapping Local Expansion Around M81 and M82 (2025), [arXiv:2510.24840 \[astro-ph.CO\]](#).

[166] A. Domínguez *et al.*, A new measurement of the Hubble constant using gamma-ray attenuation, *Astrophys. J.* **948**, 137 (2023), [arXiv:2306.09878 \[astro-ph.CO\]](#).

[167] J. Gao, Z. Zhou, M. Du, R. Zou, J. Hu, and L. Xu, A Measurement of Hubble Constant Using Cosmographic Approach from Fast Radio Bursts and SNe Ia (2023), [arXiv:2307.08285 \[astro-ph.CO\]](#).

[168] L. W. H. Fung, T. Broadhurst, and G. F. Smoot, Pure Gravitational Wave Estimation of Hubble's Constant using Neutron Star-Black Hole Mergers (2023), [arXiv:2308.02440 \[astro-ph.CO\]](#).

[169] W. Ballard, A. Palmese, I. Magaña Hernandez, *et al.*, A dark siren measurement of the Hubble constant with the LIGO/Virgo gravitational wave event GW190412 and DESI galaxies (2023), [arXiv:2311.13062 \[astro-ph.CO\]](#).

[170] V. Alfradique, C. R. Bom, A. Palmese, *et al.*, A dark siren measurement of the Hubble constant using gravitational wave events from the first three LIGO/Virgo observing runs and DELVE (2023), [arXiv:2310.13695 \[astro-ph.CO\]](#).

[171] C. Grillo *et al.*, Cosmography with supernova refsdal through time-delay cluster lensing: independent measurements of the hubble constant and geometry of the universe (2024), [arXiv:2401.10980 \[astro-ph.CO\]](#).

[172] I. Magaña Hernandez and A. Ray, Beyond Gaps and Bumps: Spectral Siren Cosmology with Non-Parametric Population Models (2024), [arXiv:2404.02522 \[astro-ph.CO\]](#).

[173] C. R. Bom, V. Alfradique, A. Palmese, *et al.*, A dark standard siren measurement of the Hubble constant following LIGO/Virgo/KAGRA O4a and previous runs (2024), [arXiv:2404.16092 \[astro-ph.CO\]](#).

[174] K. C. Wong, F. Dux, A. J. Shajib, S. H. Suyu, M. Millon, P. Mozumdar, P. R. Wells, A. Agnello, S. Birrer, E. J. Buckley-Geer, F. Courbin, C. D. Fassnacht, J. Frieman, A. Galan, H. Lin, P. J. Marshall, J. Poh, S. Schuldt, D. Sluse, and T. Treu, TDCOSMO: XVI. Measurement of the Hubble constant from the lensed quasar WGD 2038–4008, *Astronomy & Astrophysics* **689**, A168 (2024).

[175] D. H. Gao, Q. Wu, J. P. Hu, S. X. Yi, X. Zhou, F. Y. Wang, and Z. G. Dai, Measuring the hubble constant using localized and nonlocalized fast radio bursts, *Astronomy & Astrophysics* **698**, A215 (2025).

[176] T. Li, T. E. Collett, P. J. Marshall, S. Erickson, W. Enzi, L. Oldham, and D. Ballard, Correcting for selection biases in the determination of the hubble constant from time-delay cosmography (2025), [arXiv:2410.16171 \[astro-ph.CO\]](#).

[177] Z.-L. Zhang and B. Zhang, Cosmological parameter estimate from persistent radio sources of fast radio bursts, *The Astrophysical Journal Letters* **984**, L40 (2025).

[178] R. Gao, H. Gao, Z. Li, and Y.-P. Yang, *FrB cosmology with the rm-prs luminosity correlation* (2025), arXiv:2504.15119 [astro-ph.CO].

[179] S. I. Loubser *et al.*, An independent estimate of $h(z)$ at $z=0.5$ from the stellar ages of brightest cluster galaxies (2025), arXiv:2506.03836 [astro-ph.CO].

[180] Y. Liu and M. Oguri, The Hubble constant from the improved lens modeling of cluster-lensed supernova Refsdal with new spectroscopic redshifts and the Jackknife method (2025), arXiv:2509.09979 [astro-ph.CO].

[181] E. Paic, F. Courbin, C. D. Fassnacht, *et al.*, TD-COSMO. XXIV. Measurement of the Hubble constant from the doubly lensed quasar HE1104-1805 (2025), arXiv:2512.03178 [astro-ph.GA].

[182] F. Andrade-Oliveira, D. Sanchez-Cid, D. Laghi, and M. Soares-Santos, *First measurement of the hubble constant from a combined weak lensing and gravitational-wave standard siren analysis* (2026), arXiv:2601.04774 [astro-ph.CO].

[183] M. Bulla, M. W. Coughlin, S. Dhawan, and T. Dietrich, Multi-messenger constraints on the Hubble constant through combination of gravitational waves, gamma-ray bursts and kilonovae from neutron star mergers, *Mon. Not. R. Astron. Soc.* **514**, 1484 (2022), arXiv:2205.09145 [astro-ph.HE].

[184] T. Liu and K. Liao, Determining cosmological-model-independent h_0 and post-newtonian parameter with time-delay lenses and supernovae (2023), arXiv:2309.13608 [astro-ph.CO].

[185] J. E. Gonzalez, M. Ferreira, L. R. Colaço, R. F. L. Holanda, and R. C. Nunes, Unveiling the Hubble constant through galaxy cluster gas mass fractions, *Phys. Lett. B* **857**, 138982 (2024).

[186] V. K. Jaiswal, C. J. Grier, K. Horne, *et al.*, Application of the frado model of blr formation to the seyfert galaxy ngc 5548 and the first step toward determining the hubble constant, *Astrophys. J.* **964**, 78 (2024), arXiv:2410.03597 [astro-ph.GA].

[187] L. R. Colaço, R. F. L. Holanda, Z. C. Santana, and R. Silva, A joint analysis of strong lensing and type Ia supernovae to determine the Hubble constant, *Eur. Phys. J. C* **85**, 5 (2025).

[188] G.-H. Du, T.-N. Li, J.-L. Ling, Y.-H. Yao, J.-F. Zhang, and X. Zhang, Model-independent late-universe measurements of H_0 and Ω_K with the PAge-improved inverse distance ladder, arXiv (2025), arXiv:2510.26355 [astro-ph.CO].

[189] M. J. Reid, D. W. Pesce, and A. G. Riess, An Improved Distance to NGC 4258 and Its Implications for the Hubble Constant, *Astrophys. J. Lett.* **886**, L27 (2019).

[190] G. Pietrzyński *et al.*, A distance to the Large Magellanic Cloud that is precise to one per cent, *Nature* **567**, 200 (2019).

[191] S. Birrer, A. J. Shajib, A. Galan, M. Millon, T. Treu, A. Agnello, M. Auger, G. C.-F. Chen, L. Christensen, T. Collett, F. Courbin, C. D. Fassnacht, L. V. E. Koopmans, P. J. Marshall, J.-W. Park, C. E. Rusu, D. Sluse, C. Spinello, S. H. Suyu, S. Wagner-Carena, K. C. Wong, *et al.*, Tdcosmo: Iv. hierarchical time-delay cosmography – joint inference of the hubble constant and galaxy density profiles, *Astronomy & Astrophysics* **643**, A165 (2020), arXiv:2007.02941 [astro-ph.CO].

[192] P. L. Kelly *et al.*, Multiple images of a highly magnified supernova formed by an early-type cluster galaxy lens, *Science* **347**, 1123 (2015).

[193] Y.-Y. Wang, S.-P. Tang, Z.-P. Jin, and Y.-Z. Fan, The late afterglow of gw170817/grb 170817a: A large viewing angle and the shift of the hubble constant to a value more consistent with the local measurements, *The Astrophysical Journal* **943**, 13 (2023).

[194] Y.-Y. Wang, J.-P. Hu, G.-K. Zhang, and F.-Y. Wang, Hubble Constant from Localized Fast Radio Bursts, *The Astrophysical Journal* **981**, 6 (2024).

[195] D. Brout *et al.*, The Pantheon+ Analysis: Cosmological Constraints, *Astrophys. J.* **938**, 110 (2022).